Max-Planck-Institut
für Meteorologie

EXAMENSARBEIT Nr. 4

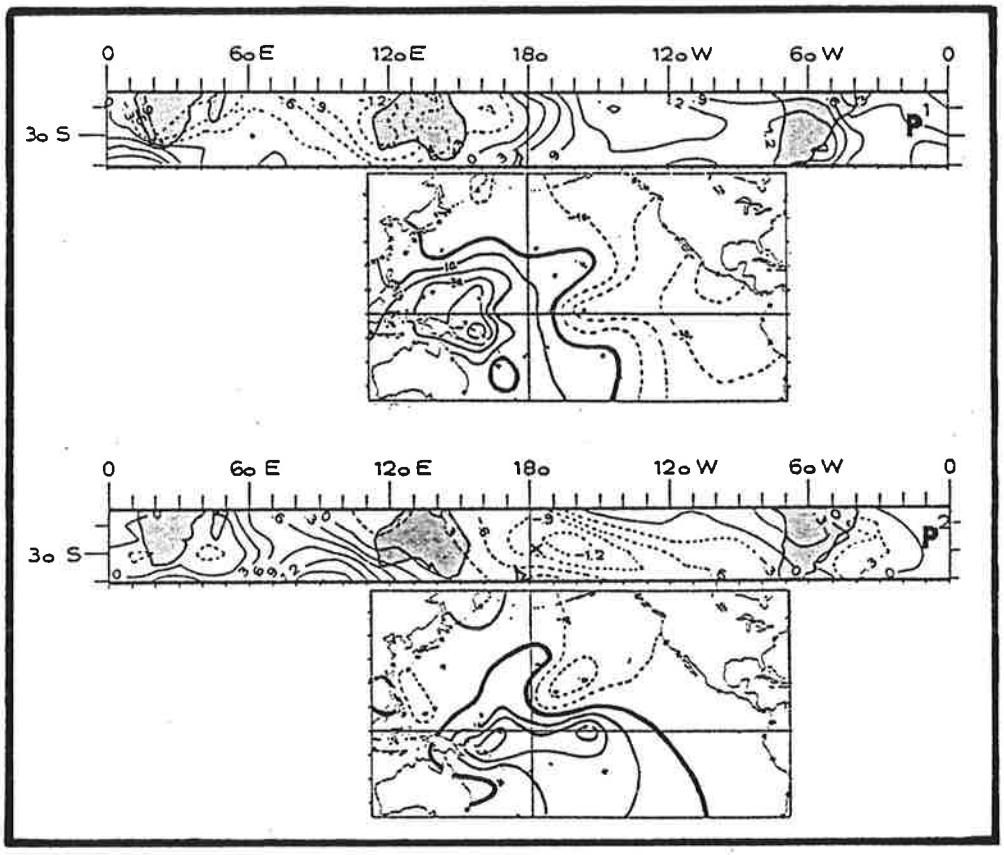

ANALYSIS AND PREDICTION OF THE EL NIÑO SOUTHERN OSCILLATION PHENOMENON USING PRINCIPAL OSCILLATION PATTERN ANALYSIS

von

JING-SONG XU

HAMBURG, AUGUST 1990

DOKTORARBEIT

AUTOR:

JING-SONG XU

MAX-PLANCK-INSTITUT
FÜR METEOROLOGIE

MAX-PLANCK-INSTITUT
FÜR METEOROLOGIE
BUNDESSTRASSE 55
D-2000 HAMBURG 13
F.R. GERMANY

Tel.: (040) 4 11 73-0
Telex: 211092
Telemail: MPI.METEOROLOGY
Telefax: (040) 4 11 73-298

EXb 4

Als Dissertation angenommen vom Fachbereich Geowissenschaften der Universität

Hamburg aufgrund der Gutachten von Prof. Dr. K. Hasselmann

und Prof. Dr. G. Fischer

Hamburg, den 4.7.1990

Prof. Dr. M. Dunst

(Sprecher des Fachbereiches Geowissenschaften)

ANALYSIS AND PREDICTION OF THE EL NIÑO SOUTHERN OSCILLATION PHENOMENON USING PRINCIPAL OSCILLATION PATTERN ANALYSIS

DISSERTATION
ZUR ERLANGUNG DES DOKTORGRADES
DER NATURWISSENSCHAFTEN IM FACHBEREICH
GEOWISSENSCHAFTEN DER UNIVERSITÄT HAMBURG

VORGELEGT VON
JIN-SONG XU
AUS PEKING, CHINA

HAMBURG 1990

CONTENTS

ABSTRACT

Principal Oscillation Pattern (POP) analysis, which is a technique for deriving the space-time characteristics of a complex system, is used for analyzing and predicting the Southern Oscillation.

Pairs of patterns are derived from the POP analysis of the Southern Hemisphere sea level pressure field and from the associated correlation pattern analysis of other atmospheric and oceanic parameters. The two vectors, that are combined from these pairs of patterns, form basis vectors of a two-dimensional space. It is shown that the dynamic process of the Southern Oscillation can be described as a damped oscillation in this reduced space. The oscillatory feature is characterized by the eastward migration of the ascending branch of the Walker Circulation and of the anomalies in the sea level and upper layer temperature.

The coefficient time series of the two basis vectors in the reduced space may be understood as a bivariate index of the Southern Oscillation, which describes both the "peak" phase and the "onset" phase of the phenomenon. Generalizing the original concept, the POP framework is used to predict this index and the traditional univariate SO index.

In a series of hindcast experiments the POP prediction scheme is tested. It turns out to be skillful for a lead time of about two seasons. In terms of the hindcast correlation the POP forecast scores better than persistence and a conventional ARMA model in forecasting the traditional SO index.

PART 0: INTRODUCTION

The phenomenon and its statistical description

The El Niño / Southern Oscillation (ENSO) phenomenon represents the largest scale pattern of natural climate variability of the atmosphere and ocean system on the time scale of several years. Its characteristic features can be summarized by the two correlation *patterns* shown in Fig.1. The first one (Fig.1a), derived by Berlage (1957), displays the atmospheric aspect of the phenomenon - the Southern Oscillation (SO). There is a strong correlation between annual air pressure anomalies reported from various meteorological stations around the world and the pressure measured at Djakarta (Indonesia). The opposite correlations in the Indonesian region and over the central and east Pacific describe a large scale mass displacement. Consistent with this mass displacement, anomalies of the trade winds and of the sea surface temperature (SST) in the central and eastern equatorial Pacific are found. This oceanic aspect of the phenomenon - the warm phase is named El Niño - is characterized in Fig.1b. It shows the correlation pattern of the monthly SST with an index which describes the mass seesaw mentioned above. Obviously the large positive SST anomalies in the central and east Pacific develop parallel to positive pressure anomalies over the Indian ocean and Australian region and to the negative pressure anomalies over the Pacific ocean shown in Fig.1a.

To monitor the Southern Oscillation, not only patterns but also indices are needed to quantify the strength of the large scale anomalies described in Fig.1. For instance, the anomalous air pressure difference between Darwin and Papeete (Tahiti), named the *Southern Oscillation Index* (SOI), is used to measure the strength of the pattern in Fig.1a; and the area-averaged SST anomaly in the central or east Pacific is used to measure the strength of the pattern in Fig.1b. The two indices are almost equivalent (Wright, 1984).

The state that is associated with above-normal pressure in the Indonesian region and with above normal SST in the eastern Pacific is usually called a *Warm Event*. The opposite state, with below normal air pressure and colder than normal SST, is called a *Cold Event*. In the following the entire phenomenon, i.e. Cold Events and Warm Events, is denoted as the Southern Oscillation (SO).

The phenomenon under consideration is involved in the global atmosphere -

a

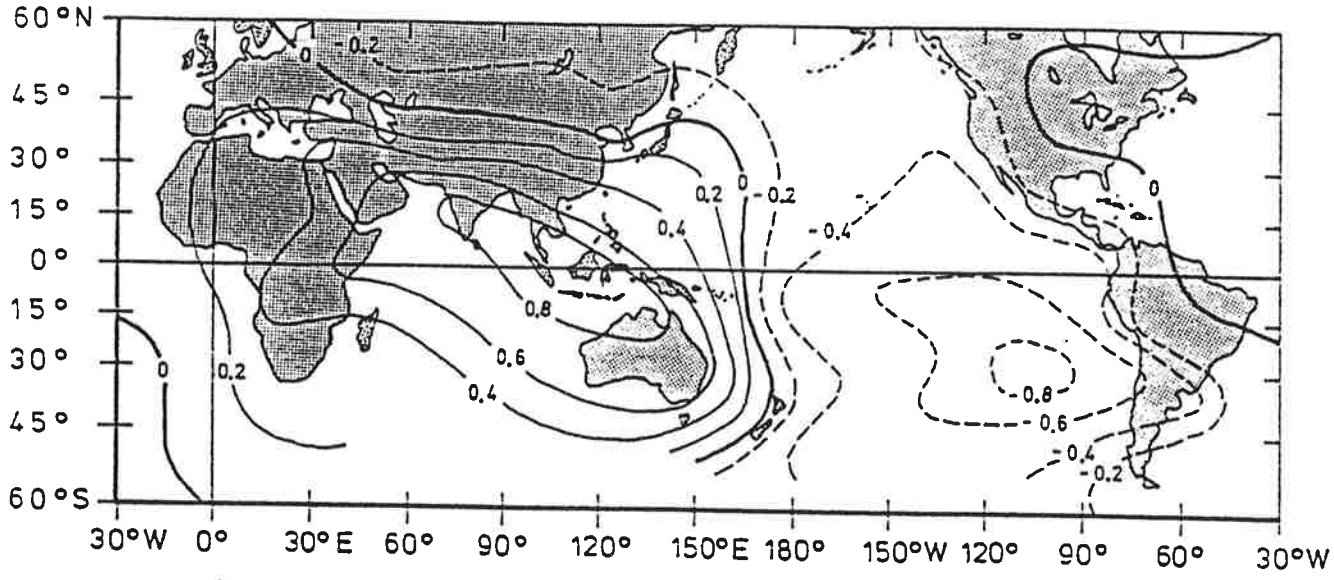

b

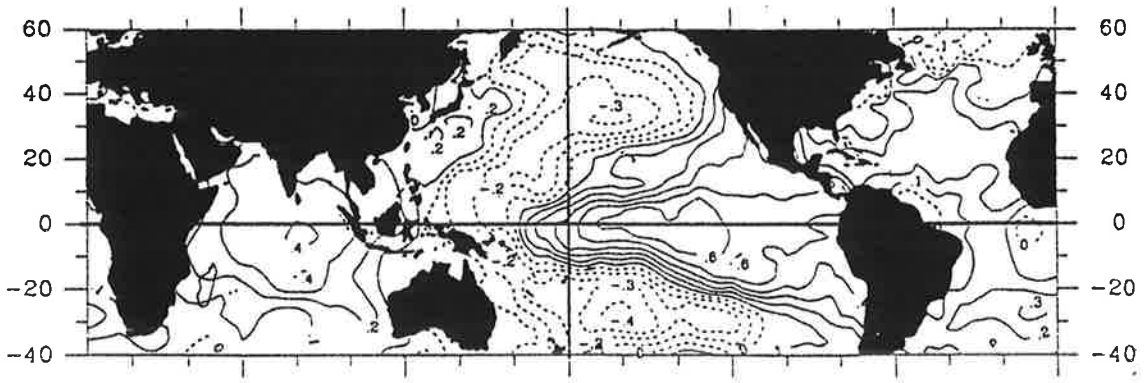

Figure 1:

a) Correlation of annual air pressure anomalies reported from various meteorological stations around the world with the pressure measured at Djakarta (Indonesia) (from Berlage, 1957).
b) Correlation of the monthly sea surface temperature anomalies with SOI.

ocean system (Bjerknes, 1966). The first problem with investigating such a complex system is its large number of degrees of freedom. Hasselmann (1988) was the first to propose a statistical strategy to derive simpler systems which contain only a few degrees of freedom but nevertheless succeed in capturing the principal *dynamic* properties of the full system. After Hasselmann (1988), it is often reasonable to assume that the system considered here can be characterized by a few patterns like those of patterns in Fig.1, and that the dynamic behavior of the system appears to be dominated by interactions between these patterns. This technique is known as Principal Interaction Pattern (PIP) analysis.

A linearization of the PIP analysis was introduced by Hasselmann (1988) and Storch et al. (1989), and denoted as Principal Oscillation Pattern (POP) analysis. In this case the system is projected mostly onto two patterns. The interaction between the patterns is simply described by a damped oscillation. It means that the dynamic behavior of the system can be approximated, at least initially, by an oscillatory development of the reduced system.

In this paper, it will be shown that the atmosphere - ocean system on time scales of several years can be considered to be projected onto two patterns. One describes the extreme situation of the Southern Oscillation, like the patterns in Fig.1; the other describes the intervening stage, or in other words, the features that characterize the transition from one extreme to the other one. Once such a reduced system has been derived from all available meteorological and oceanographic variables, an investigation of these patterns could help us to understand the air-sea interaction during the extreme stage *and* during the intervening stage, and perhaps also the origin of this low-frequency phenomenon in the atmosphere - ocean system.

Hypotheses of ENSO generation

The development of a Warm Event is generally attributed to large - scale air - sea interactions (first suggested by Bjerknes (1966), (1969)). In the normal state, the tropical Pacific is warmer in the west and colder in the east. East of the warmer region, the easterly trade winds blowing towards the atmospheric heating area drive warm surface water to the west, while drawing colder

sub-surface water upward in the east. Before a Warm Event, Kelvin waves or anomalous eastward surface currents are observed, that cause eastward migration of the warm water from the west Pacific into the central and east Pacific. Once positive SST anomalies exist over the central and east Pacific, the surface winds slacken. As a result, more warm western water moves eastward and less cold water is drawn upwards, so the east becomes warmer still. A Warm Event appears.

The further questions, how is the eastward migration of the warm water initiated and when is it active for the low frequency fluctuations of the coupled system, have led to the development of two groups of hypotheses. One, from the oceanographic point of view, stresses the dominant role of the tropical Pacific Ocean. The random atmospheric disturbances can release eastward propagating Kelvin waves, but the whole development is determined by the oceanic thermal and dynamic state. The atmospheric component is important only in amplifying the oceanic anomalies via air-sea interaction. The other group, however, suggests that the eastward migration of the warm water is generated by westerly wind anomalies, which are a result of systematic development of atmospheric circulations. The two groups agree regarding the air - sea interaction in amplification disturbances, but disagree in the role of the ocean and atmosphere in controlling the low-frequency evolution of the atmosphere - ocean system.

a) The determinant role of the ocean

The pioneer hypothesis of El Niño genesis was suggested by Wyrtki (1977, 1979, 1985), and supported by results of a coupled model (Cane, et al., 1986). They assume that the thermal state of the ocean controls the whole evolution of the coupled system. During periods when atmospheric circulation in the tropics is developed with normal strength, the trade winds push warm water towards the west and cause it to accumulate in the west Pacific. The resulting effect is a depression of the thermocline and an increase of the ocean temperature in the upper layer. High - frequency, but spatially - coherent fluctuations of the atmospheric circulation over the tropics cause a massive eastward displacement of the accumulated warm water along the equator. The warm water surging to the east is reflected at the coast of America to both north and south and is lost from the tropical ocean. A complete El Niño cycle results in a net heat

discharge from the tropical Pacific, and therefore another El Niño event could not take place until the warm water reservoir is refilled in the west Pacific.

More recently the oscillatory mode in the Pacific Ocean has been investigated. Suarez and Schopf (1989), and later other authors, proposed a delayed action oscillator model for the ENSO phenomenon. According to their model, the ENSO cycle is maintained by oceanic waves. Suarez and Schopf studied in their simplified model the relative importance of the local effect (caused by air/sea interaction) and the delayed oceanic wave effects (caused by westward off-equatorial Rossby waves and the reflected eastward equatorial Kelvin waves) and the ratio of a wave transit time to the e-folding time of the underlying coupled instability. They concluded that the slowly westward propagating Rossby waves and the eastward propagating Kelvin waves reflected at the western boundary are crucial in generating oscillatory solutions.

Battisti and Hirst (1989) investigated a similar coupled model to that of Cane et al. and found that the delayed action oscillator mode is the dominant mechanism which describes the nature of the interannual variability in the coupled system.

b) The determinant role of the atmosphere

Another group of people has investigated the determinant role of the atmosphere. Two hypotheses considered here concentrate on the possible processes of generating westerly wind anomalies. One is concerned with the Asian summer Monsoon and processes that are associated with the variability of the Asian summer Monsoon , the other with anomalies over the Southern Pacific Convergence Zone (SPCZ).

The relationship between a poor Asian summer monsoon and ENSO is evident (Mooley and Parthasarathy, 1983). It is speculated that the anomalous atmospheric circulation associated with a poor Asian summer monsoon could modify the tropical Walker Circulation, so that westerly wind anomalies would be released in the western Pacific.

The variability of the Asian summer monsoon system has been studied for more than a century. Blandford (1884) was one of the first to suggest that the

summer monsoon over India and Burma might be influenced by the spring snow cover on the Himalayas. This suggestion is based on the idea that the monsoon system is driven by the combination of land-sea temperature contrast and latent heat release. The validity of this idea has been recently supported by numerical model results (Barnett et al.1989). Barnett et al. could demonstrate that the remote near - surface atmospheric response induced by snow cover/monsoon perturbation (doubled snowfall rate) was characterized by large westerly wind anomalies over the west and central Pacific, and these were able to produce tropical Pacific SST anomalies resembling those of El Niño.

According to these numerical model results and to results of a previous study of the global sea level pressure field (Barnett, 1985), Barnett suggested that the Southern Oscillation and the Indian monsoon are part of a global-scale eastward propagating mode in the sea level pressure (SLP) field. It indicates that the Southern Oscillation is simply the consequence of the systematic development of the atmospheric circulation.

The further question of how the snow anomalies are generated was studied by Graf (1989). An atmospheric General Circulation Model (GCM) was used to test his hypothesis that a radiation deficit in polar northern latitudes, representing the effects of volcanic eruptions or polar stratospheric clouds, may generate conditions favorable for a weak Asian summer monsoon and for triggering El Niño events. The results provide physically-consistent evidence in support of his hypothesis.

The importance of the anomalies over the Southern Pacific Convergence Zone and its role in generating initial conditions for a Warm Event was suggested by van Loon and Shea (1985, 1987). They investigated the sea-air interaction in the region of the SPCZ. In the southern winter one year before a Warm Event, the subtropical high is stronger and the pressure over Australia is lower than normal. The anomalous wind associated with this pressure pattern has a strong northerly wind component, which tends to generate positive SST anomalies in the SPCZ region. In the following season the SPCZ begins to strengthen and move southward. The already generated positive SST anomalies lead then to an intensification of the convective activity in the SPCZ region which is associated with a pressure drop in that region and westerly wind anomalies over the tropical west Pacific. The later could release Warm Event.

The status of ENSO prediction

A few groups are now actively making operational predictions of the state of ENSO, as summarized by Barnett et al. (1988). The simplest model uses a statistical approach to find the optimal linear combination of variations in space and time in the zonal wind stress over the tropical Pacific, or the global sea level pressure (SLP) field that can forecast the subsequent SST change (Graham et al., 1987a and Graham et al., 1987b). The second approach is an ocean model (Busalacchi and O'Brien, 1981) which treats the tropical Pacific as a light (warm) dynamical upper layer overlying a heavy (cold) lower layer that is at rest. The model is driven with the observed wind. Forecasts are made by assuming that the wind fields in the future will be identical to that at the initialization time, i. e. the memory is basically provided by the ocean. A more realistic forecast scheme is based on the coupled model of Zebiak and Cane (1987) and consists of an ocean model similar to Busalacchi and O'Brien's and a steady-state atmosphere model. In this model the SST anomalies are primarily dynamically forced by surface wind stress anomalies, which are calculated as the response to SST anomalies. The initial state of this coupled model is estimated similarly as for the ocean model of Busalacchi and O'Brien. However, after that stage both the atmosphere and ocean evolve as solely determined by the dynamics of the coupled model.

The success of all models in predicting the 1986-87 El Niño event indicates, after the authors, that "ENSO is a long-period cycle: the coupled ocean-atmosphere system travels on a closed trajectory through a multidimensional phase space that is largely determined by its large-scale, low frequency behavior". All forecast schemes show higher skill in late summer to winter, lower skill in spring to early summer.

Purpose of this paper

In this study the Southern Oscillation phenomenon is investigated using the POP analysis, which provides a simplified description of the dynamical processes in a low-dimensional space. The first goal is to identify the low-dimensional space in which the coupled atmosphere-ocean system travels. An investigation of the system's evolution along the trajectory in the reduced

space may yield clues on the validity of the different hypotheses mentioned above, and therefore allow a more complete description of the Southern Oscillation.

The second purpose is to design a forecast scheme for the Southern Oscillation. This scheme exploits the notion of a well-defined trajectory in a low-dimensional space. After having identified the location on the trajectory at a certain time, the future state, that is travelling along the trajectory, can be predicted within some range of uncertainty.

The paper is organized into five parts. The first part describes the POP analysis method and the POP prediction scheme. Then, in part II, a two-dimensional space is derived from a basic data set. The dynamical behavior of the atmosphere-ocean system in this two-dimensional space is investigated and described in part III. Part IV demonstrates the skill of the POP prediction scheme by presenting some case studies and by deriving a measure of skill in a series of hindcast experiments. The results of the previous parts are discussed and concluded in the final part V with respect to the physical mechanisms of the SO and its predictability.

PART I: CONCEPTS OF POP ANALYSIS AND POP PREDICTION

1. POP ANALYSIS AND THE ASSOCIATED CORRELATION PATTERN ANALYSIS

POP (Principal Oscillation Pattern) analysis is a technique to extract regularly developing (e.g., oscillating or standing) spatial patterns from a multi-component system whose dynamics are unknown or too complex to be easily described (Storch et al. 1988). Conceptually, POP analysis represents a simplification of the Principal Interaction Pattern analysis (PIP) (Hasselmann, 1988). Alternatively POP analysis may be thought of as a normal mode analysis using an estimated system matrix. In the following I will describe the latter approach briefly. More details are given by Storch et al. (1988, 1989a).

In order to focus on specific time scales, the vector time series to be analyzed is filtered in time and space, retaining variability only on the temporal and spatial scales of interest. The filtered time series, $\mathbf{x}(t)$, is then assumed to be generated by a first-order multivariate autoregressive process:

$$\mathbf{x}(t+1) = A\,\mathbf{x}(t) + \text{forcing} \tag{1}$$

If the forcing in (1) is uncorrelated with $\mathbf{x}(t)$, an estimate of the matrix A may be obtained in two different ways. One way is to multiply (1) from the right with the transpose of $\mathbf{x}(t)$ and to take expectations. The other way is to find a matrix A which minimizes $\langle(\mathbf{x}(t+1) - A\,\mathbf{x}(t))^2\rangle$. In both cases the result is $A = C_1 \cdot C_0^{-1}$ with C_1 and C_0 denoting the lag-1 and lag-0 covariance matrices of $\mathbf{x}(t)$. The matrices C_1 and C_0 are estimated in the conventional manner.

Generally, the matrix A is not symmetric, and thus its eigenvectors P and eigenvalues λ are not all real. Some may occur in pairs of conjugate complex eigenvectors, $\mathbf{P}^2 \pm i\mathbf{P}^1$, and eigenvalues, $\lambda^2 \pm i\lambda^1$. The (real or complex) eigenvectors are called POPs of the time series $\mathbf{x}(t)$. In most cases, the eigenvectors are linearly independent so that the state $\mathbf{x}(t)$ may uniquely be written as:

$$\mathbf{x}(t) = \sum_{\substack{j \\ \text{all POPs}}}^{\text{real}} z_j(t)\,\mathbf{P}_j + \sum_{\substack{j \\ \text{all POPs}}}^{\text{complex}} (z_j^1(t)\,\mathbf{P}_j^1 + z_j^2(t)\,\mathbf{P}_j^2) + \text{forcing} \tag{2}$$

with real time coefficients $z(t)$ for real POPs and complex time coefficients $z(t)$ with imaginary part $z^1(t)$ and real part $z^2(t)$ for complex POPs. The

coefficients may be obtained by taking the dot product of the vector $\mathbf{x}(t)$ and the adjoint eigenvector D (the matrix of adjoint eigenvectors $D_{ADJ.}=(D_1|D_2\cdots|D_n)$ is given by $D_{ADJ.}=(P_{POP}^{-1})^T$, where T denotes transposition, and $P_{POP}=(P_1|P_2\cdots|P_n)$ is the matrix of eigenvectors of A)

The coefficient time series of a considered POP satisfies

$$z(t_o+t) = \lambda^{t^*} z(t_o) + \text{forcing} \qquad (3)$$

where λ is the eigenvalue of the POP. For a real POP, $z(t)$ and λ are also real. (3) describes an exponential dampening of the initial signal. For a complex POP, $z(t)$ and λ are complex with $\lambda= |\lambda|e^{i\phi}$. (3) describes in this case a damped oscillation. The e-folding time τ and the oscillation period T are derived from the eigenvalue λ:

$$\tau = -1/\ln|\lambda| \qquad (4)$$

$$T = \frac{2\pi}{\phi}$$

Because of the particular form of (3), the real - valued POPs are called standing patterns and the complex - valued POPs *oscillatory* patterns. An oscillatory pattern often describes a feature that migrates in space. This is particularly true if the imaginary part, P^1, and the real part, P^2, are spatially in quadrature.

The error, $e(t) = \mathbf{x}(t) - z(t)\cdot\mathbf{P}$ or $e(t) = \mathbf{x}(t) - z^1(t)\cdot P^1 - z^2(t)\cdot P^2$, in reproducing $\mathbf{x}(t)$ using only one standing real POP P or one oscillatory complex POP P^2+iP^1 may be conveniently measured by the skill parameter

$$S^r = 1 - \frac{\langle e^2\rangle}{\langle x^2\rangle} \qquad (5)$$

where $\langle\ \rangle$ denotes expectation. $S^r=0$ indicates that the POP model has no skill, whereas $S^r=1$ indicates perfect skill.

After having identified a certain POP in the "key variable" $\mathbf{x}(t)$, it is often desirable to describe the signal in terms of other simultaneously observed variables $\mathbf{v}(t)$, e.g., SST. To do this we use "associated correlation patterns". In the case of an oscillatory mode these patterns, denoted by Q_v^1

and Q_v^2, are defined to minimize

$$(6) \qquad < \| v(t) - \frac{z^1(t)}{\sigma^1} Q_v^1 - \frac{z^2(t)}{\sigma^2} Q_v^2 \| >$$

where $\| \|$ denotes a quadratic norm. The coefficients $z^1(t)$ and $z^2(t)$ of the considered POP in the variable **x**, are divided by their standard deviations, σ^1 and σ^2, in order to convert the patterns into the same units as the field **v**.

In the case of oscillatory patterns, the POP model can be interpreted as the system's tendency to generate a damped oscillation with parallel evolutions of **x**(t) and **v**(t) as follows:

for **x**(t): $\ldots \rightarrow P^1 \rightarrow P^2 \rightarrow -P^1 \rightarrow -P^2 \rightarrow P^1 \rightarrow \ldots$

for **v**(t): $\ldots \rightarrow Q_v^1 \rightarrow Q_v^2 \rightarrow -Q_v^1 \rightarrow -Q_v^1 \rightarrow Q^2{}_v \rightarrow \ldots$

where P^2/Q_V^2 replaces P^1/Q_V^1 after quarter of period, $-P^1/-Q_V^1$ replaces P^2/Q_V^2 after an other quarter of period, and so on.

2. THE POP PREDICTION SCHEME

For the sake of brevity, I consider only oscillatory, i.e. complex - valued, POPs in this section. For standing patterns, the scheme takes a similar form.

Let us assume that a relevant oscillatory POP, P^2+iP^1, has been identified. Its state at a certain time t_o is measured by the complex coefficient $z(t_o) = z^2(t_o) + iz^1(t_o)$. Its future state, $z(t_o+t)$, would be known if the forcing in (3) were known. Obviously, the forcing describes all processes which cannot be treated in the linear scheme (1). Thus the forcing is considered to be unpredictable noise and the future state $\hat{z}(t)$ is predicted from

$$(7) \qquad \left[\hat{z}^1(t_o+t) + i\hat{z}^2(t_o+t) \right] = \left(|\lambda| \, e^{-\frac{2\pi i}{T}} \right)^t \left[z^1(t_o) + iz^2(t_o) \right]$$

which is obtained from (3) by neglecting the forcing. Thus the prediction problem is reduced to estimating the initial value $z(t_o)$.

If the raw data are not filtered in time, the estimation is straightforward. First, the data are filtered in space, if necessary, and then the time coefficient is calculated using the adjoint patterns. In the hindcast experiments in this study, however, the data are noisy and have to be smoothed before the initial value is estimated. For this purpose a non-symmetric time domain filter is applied (see Appendix), which approximates the spectral characteristics of the frequency domain filter used in the POP analysis.

The time evolution of the process to be described by a complex POP may conveniently be represented in the two-dimensional z-plane. Utilizing (3), or (7), the z(t) trajectory normally rotates clockwise around the origin. Its magnitude may be described by the *S*-distance, d(z), of z(t) from the origin:

$$(8) \qquad d(z) = z^T \cdot S^{-1} \cdot z$$

with *S* being the covariance matrix ($<z^j z^k>$) of z. If z is normally distributed with zero mean, the *S*-distance d(z) is χ^2-distributed. z(t) is considered to be "small", or "very large", if $d(z) \le b_1$ or $d(z) \ge b_2$ with some appropriate numbers b_1 and b_2. If z is small, the process described by the POP pair is interpreted as being in a "quiet" phase. If z is not small, the process is "active"; if it is very large the process is "strongly active".

In this study the SO is divided into three classes of states of equal likelihood: a quiet phase , and warm and cold phases. The latter two phases comprise the active stage, and the strongest 10% of all states are considered as being strongly active. Therefore the critical values b_1 and b_2 are chosen so that $Prob\{d(z) \leq b_1\} < 33\%$ and $Prob\{d(z) \geq b_2\} < 10\%$.

To assess the proposed POP scheme's predictive capabilities, the outcome of a series of hindcast experiments can be compared with a traditional reference, the persistence forecast (Livezey, 1987), and a conventional univariate ARMA process (Chu and Katz, 1985). To do this, a univariate prediction skill is required:

$$S^P = \frac{\langle O \cdot P_\tau \rangle}{\sqrt{\langle O^2 \rangle \langle P_\tau^2 \rangle}} \tag{9}$$

where $O(t)$ and $P_\tau(t)$ are statistics of the observed, and predicted at lag τ, parameters respectively. If this statistic is perfectly predicted, $S^P=1$, whereas $S^P=0$ for a useless prediction. S^P is certainly not the optimal measure to compare two sets of hindcasts. In particular, it is not sensitive to systematic errors in the strength of the predicted signal, so that the persistence forecast and damped persistence forecast yield identical skills S^P.

3. COMPARISON WITH OTHER STATISTICAL TECHNIQUES

The statistical techniques used in climate research can be divided into two classes. One is based on classical time series analysis, and is concerned with the building of stochastic models that describe temporal evolution of a univariate time series; the other is the concept of Empirical Orthogonal Functions (EOFs) (Preisendorfer, 1988), which concentrate on the covariance structure of fields.

The stochastic models for univariate time series are often autoregressive and moving average (ARMA) processes. A process which is suitable for the considered time series may tell us something about the nature of the system generating the time series, and could also be used for obtaining forecasts of the future values of the time series. However the phenomenon under consideration develops inhomogeneity in a multicomponent space comprising both atmosphere and ocean. A modeling of one particular time series in such a complex system can certainly not capture the large scale dynamical processes. This disadvantage of the univariate ARMA processes is demonstrated again in Part IV.

The EOF analysis, on the other hand, is designed to yield an optimal representation of the covariance structure of *fields*. In the case of conventional EOFs, simultaneous covariances are considered and the spatial patterns represent orthogonal standing features. With *extended EOFs*, lagged covariances are also taken into account so that it is possible to describe time-dependent spatial patterns. In the *complex EOF analysis* the eigenvalues and eigenvectors of the cross - spectral matrix averaged over a certain frequency band are derived. The resulting complex eigenvectors may be used to describe oscillatory behavior in space. In all cases, the EOF analysis leads to patterns which maximize variances. The eigenvalues represent the amount of variance explained by the patterns. If characteristic numbers of the temporal behavior are desired, these have to be inferred by, e.g., cross - spectral analysis of the EOF coefficients.

In contrast to EOFs, the POPs do not form a set of orthogonal patterns so that the POP coefficients are not given as the dot product of the patterns with the

field to be analyzed but as the dot product of this field with the adjoint patterns. Also the POP coefficients are not necessarily mutually independent as the EOF coefficients are. Dynamically this lack of independence is not disadvantageous; there is no a-priori reason why different processes, identified by POPs, should be statistically independent. Another difference from the EOFs is that the POP analysis yields no information on the amount of variance connected with individual POPs. The explained variance, which is not maximized by the POPs, has to be calculated explicitly from the data.

To conclude: The main difference between the POP technique and any other EOF technique is that the latter maximizes variances whereas the former explicitly specifies a dynamical model (1). In contrast to the univariate ARMA processes, the specified model is derived from a multivariate time series, so that the spatial evolution of a dynamical process is captured by the POP analysis.

4. APPLICATION OF POP ANALYSIS TO A COMPLEX SYSTEM

In the hope of getting a comprehensive picture of the Southern Oscillation, data from various sources are considered in this study. Principally there are two different, and almost equivalent, ways to apply the POP analysis to a data set combined from a series of subsets. The first way is to POP - analyze the entire data set. The second possibility is to POP - analyze only one subset, noted as the *key variable*, and then using the associated correlation pattern analysis for the other subsets. The former shows limited capacity in capturing the dominant feature of the considered phenomenon if the signal-to-noise level is low in some subsets. The latter, on the other hand, avoids this problem by limiting the POP analysis to a key variable, which has a large signal-to-noise level. The description of the signal in the entire data set by the associated correlation patterns, and the quantification of its relevance in each subset in terms of explained variance, allows for a better separation between the signal and the noise. In both cases, when one relevant POP pair is found, the complex system $\mathbf{x}(t)$ can than be reduced to a two-dimensional space spanned by two vectors. In the first case, these vectors are P_x^1, P_x^2; in the second case they are $\begin{pmatrix} P_x^1 \\ Q_v^1 \end{pmatrix}$, $\begin{pmatrix} P_x^1 \\ Q_v^1 \end{pmatrix}$ with P_x^1, P_x^2 being the POP pair derived from $\mathbf{x}(t)$ and Q_v^1, Q_v^2 being the associated correlation patterns for the variable $\mathbf{v}(t)$. The temporal evolution is described by eq.(3), i.e. it displays a damped oscillation in the reduced system.

The key variable does not need to contain the full signal, but it must contain at least an important part of the signal. This problem is demonstrated by the example of 30-60 day waves (Storch and Xu, 1989). The POP analysis of the equatorial velocity potential at 200-mb leads to the concept that the tropical 30- to 60-day wave has a zonal wave number 1 pattern, which travels once around the equator in 30 to 60 days. The oscillation is strong and propagates slowly in the convectively active equatorial areas (over the tropical Indian ocean and the Indonesia region). When the analysis was restricted to part of the equator, e.g. the area over the equatorial Indian Ocean or the Indonesia region only, the space-time characteristics were also identified by this reduced subset of data. The signal identified by the POP analysis became weak and vague, however, when an area was considered in which the signal is not strong, for example at extratropical latitudes, or in the less convectively

active western Pacific.

It is noted that the technique, i.e. the POP analysis of the key variable and the associated correlation pattern analysis of the other subsets, does not determine the dominant role of the key variable in the considered process.

PART II: THE POP MODEL OF THE SOUTHERN OSCILLATION

5. THE KEY VARIABLE

The key variable for investigating the Southern Oscillation has to satisfy three conditions. First of all the key variable should contain an important part, but not necessarily the whole of the evolution of the signal. Secondly, because of the predictive purpose the key variable should be an operational data set. Thirdly, to perform the fit of the POP model, it is necessary to have long time series available. Fig.1a shows that sea level pressure describes large SO related variabilities, whose maximum is located in the tropics and subtropical Southern Hemisphere. Since operational analyses of tropical SLP are not available prior to 1979, it is reasonable to choose the operational Southern Hemisphere (south of 10°S) sea level pressure (SLP) analysis from Australian Weather Service as the key variable in this study.

The Southern Hemisphere monthly mean SLP, used as the key variable, covers the area from 15°S to 40°S. The data come from two periods: the first extends from January 1951 to December 1958 (South Africa Weather Service), and the second extends from April 1972 to September 1988 (Australian Bureau of Meteorology).

Prior to the POP analysis, the SLP data are processed as follows:

- The anomaly fields are calculated separately for the two periods 1951-58 and 1972-83 in order to remove long term trends (Mo and van Loon, 1985) and possible inhomogeneities of the data sets.
- At each grid point, the time series are normalized by the local standard deviation. This procedure is necessary because of the considerable difference in variability of the mid-latitude SLP and the subtropical SLP.
- All variance on time scales shorter than 15 months is filtered out and all variance on time scales greater than 18 months is retained unaltered (see Appendix). The characteristics of the filter have been chosen to focus on the SO phenomenon, which has a typical time scale of the order of 3 to 4 years.

  The time filtering did not take into account the 1959-71 gap between the data sets. This is reasonable when estimating the statistical parameters: The data are noisy, and the sole effect of the sudden 1959/71 jump is to slightly distort the spectral estimates.
- The time-filtered data are projected onto the subspace spanned by the first 9 EOFs, which explain 85% of the total variance. Some experiments were made

to address the sensitivity of the results to the number of EOFs used. It turned out that the results were stable if at least the first 9 EOFs were used.

The aim of the POP analysis is to identify a low-dimensional space in which the bulk of the dynamical process of the Southern Oscillation is taking place. In such a reduced space, at least one basis vector should characterize the extremes of the Southern Oscillation, i.e. the coefficient time series of this basis vector should be coherent with the traditional Southern Oscillation Index (SOI, defined as pressure difference between Darwin and Papeete). There is therefore a good reason to compare the results of the POP analysis with the traditional SOI as an initial verification. The SOI is filtered in the same way as the SLP data.

6. RESULTS OF THE POP ANALYSIS FOR THE KEY VARIABLE

One relevant oscillatory POP pair is found in the Southern Hemisphere SLP data. Its oscillation period T is about 37 months and its e-folding time τ is about 47 months. The explained variance S^r of this POP pair is 16% for the entire subtropical Southern Hemisphere SLP time series.

The POP coefficient time series, $z^1(t)$ and $z^2(t)$, are presented in Fig.2a. The filtered SOI derived from the gridded SLP field (solid line) and the station data (dashed line) are shown in Fig.2b. The large difference between the two curves in Fig.2b in the early fifties indicates that the quality of the SLP field is poor in that period. Generally the minima (maxima) of the filtered SOI in 1951, 53, 57/58, 72, 76/77, 82/83 and 87 (1955/56, 73/74, 75 and 88) correspond with Warm (Cold) Events. The artificial filter effect is visible in the three examples, 1976/77, 1981 and 1988. The unfiltered SOI shows two minima at the ends of 1976 and 1977. However, the one in 1977 is larger, and causes one broad minimum in 1977 in the filtered time series. Compared with the unfiltered SOI, the maximum in 1981 is slightly overestimated because of large negative values in 1982/83. The maximum in 1988 on the other hand is underestimated because of the filter effect at the end of the time series.

In the years of Warm Events 1951, 53, 57/58, 72, 76/77, 82/83 and 87 (Cold Events 1955/56, 73/74, 75 and 88), when the SOI is minimum (maximum) the coefficient $z^1(t)$ is generally also minimum (maximum) almost simultaneously, and $z^2(t)$ is minimum (maximum) several months later. It seems that in years of "Events" the two time series show oscillatory behavior. The oscillation period varies between 2 and 3 years. The results of cross - spectral analysis of the POP coefficients and the SOI (Fig.3) substantiate these impressions. The coherencies (Fig.3a) between each two time series, $z^1(t)$, $z^2(t)$ and SOI, are high on the time scale of 2-3 years (significantly nonzero at a level of more than 99%). Maximum coherence is obtained for 30 months. The phase relationship between these three time series are demonstrated in Fig.3b. $z^1(t)$ and $z^2(t)$ are 90° out-of-phase, with $z^1(t)$ leading $z^2(t)$. $z^1(t)$ leads the SOI by about 2 months, and $z^2(t)$ lags the SOI by about 7 months, when the oscillation period of about 30 months is considered.

The POPs are shown in Fig. 4. The pattern P^1 has large positive anomalies over

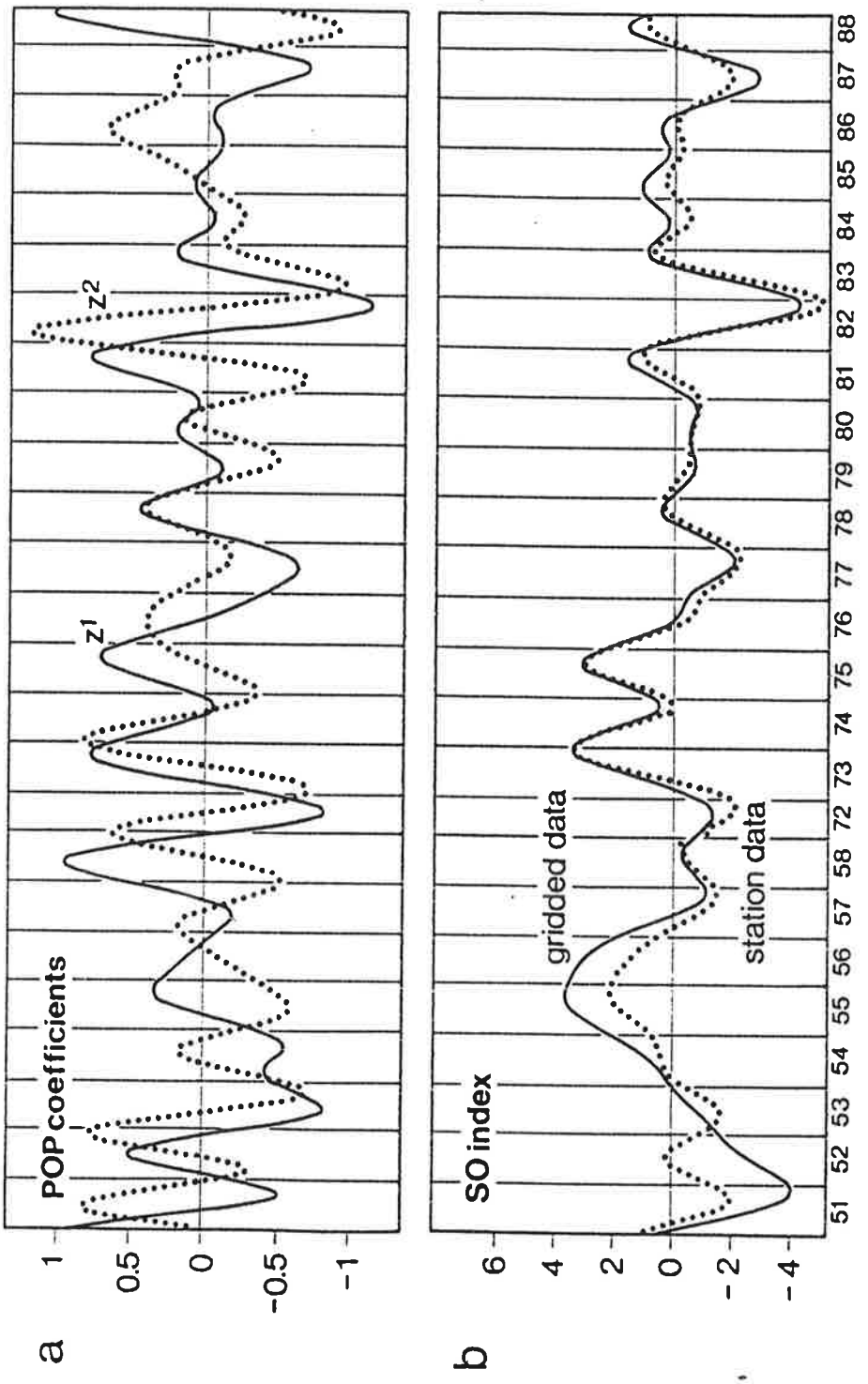

Figure 2:
Time series of
a) POP coefficients $z^1(t)$ (heavy) and $z^2(t)$ (light). The coefficients are dimensionless.
b) Southern Oscillation Index "Darwin minus Papeete SLP" as derived from station data (solid) and analyzed gridpoint data (light; prepared by the South African Weather Service (1951-58) and the Australian Bureau of Meteorology (1972 to 88)). Note the large differences in the 1950s.
The curves are time-filtered. Units: mb.

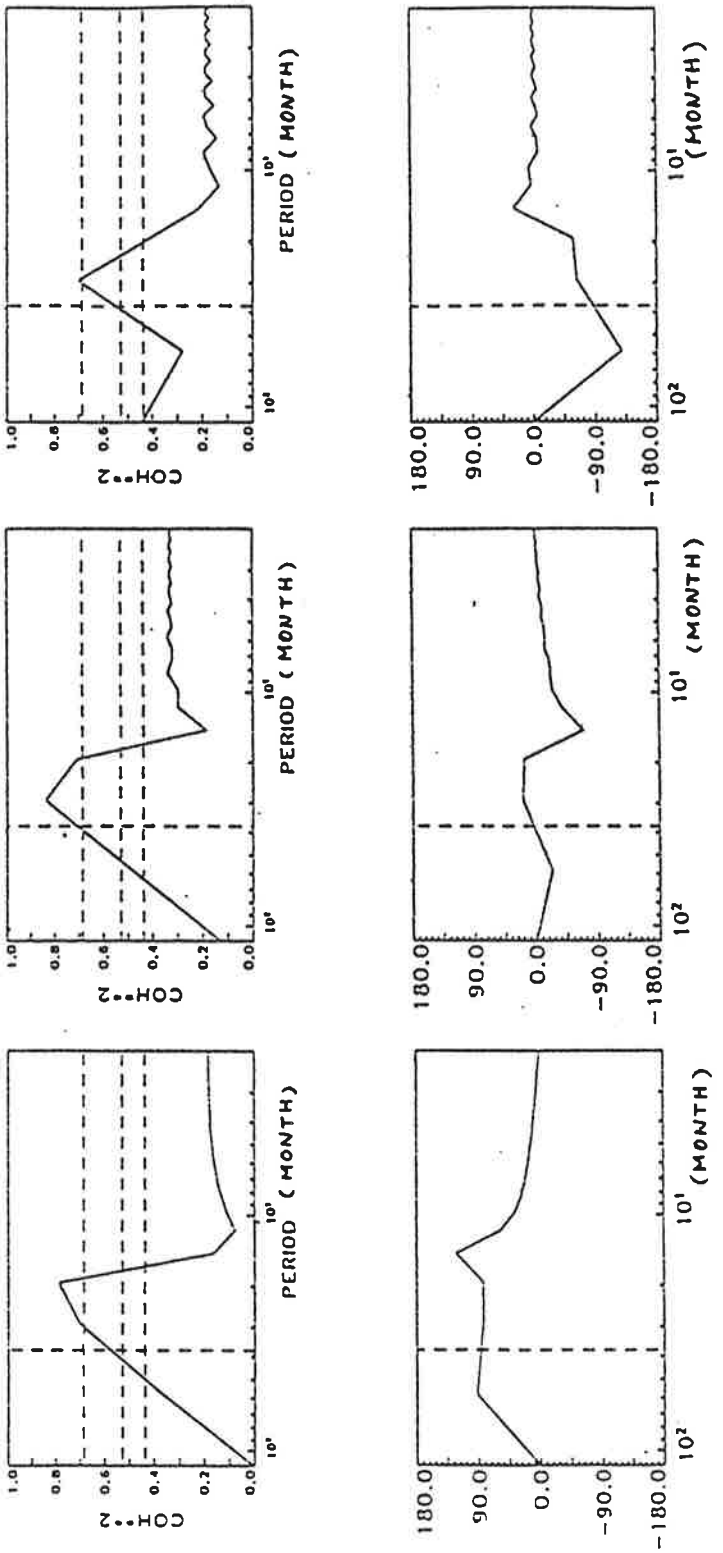

Figure 3:
a) Coherence spectrum between time series $z^1(t)$ and $z^2(t)$, $z^1(t)$ and SOI, and $z^2(t)$ and SOI.
b) Phase spectrum between time series $z^1(t)$ and $z^2(t)$, $z^1(t)$ and SOI, and $z^2(t)$ and SOI.

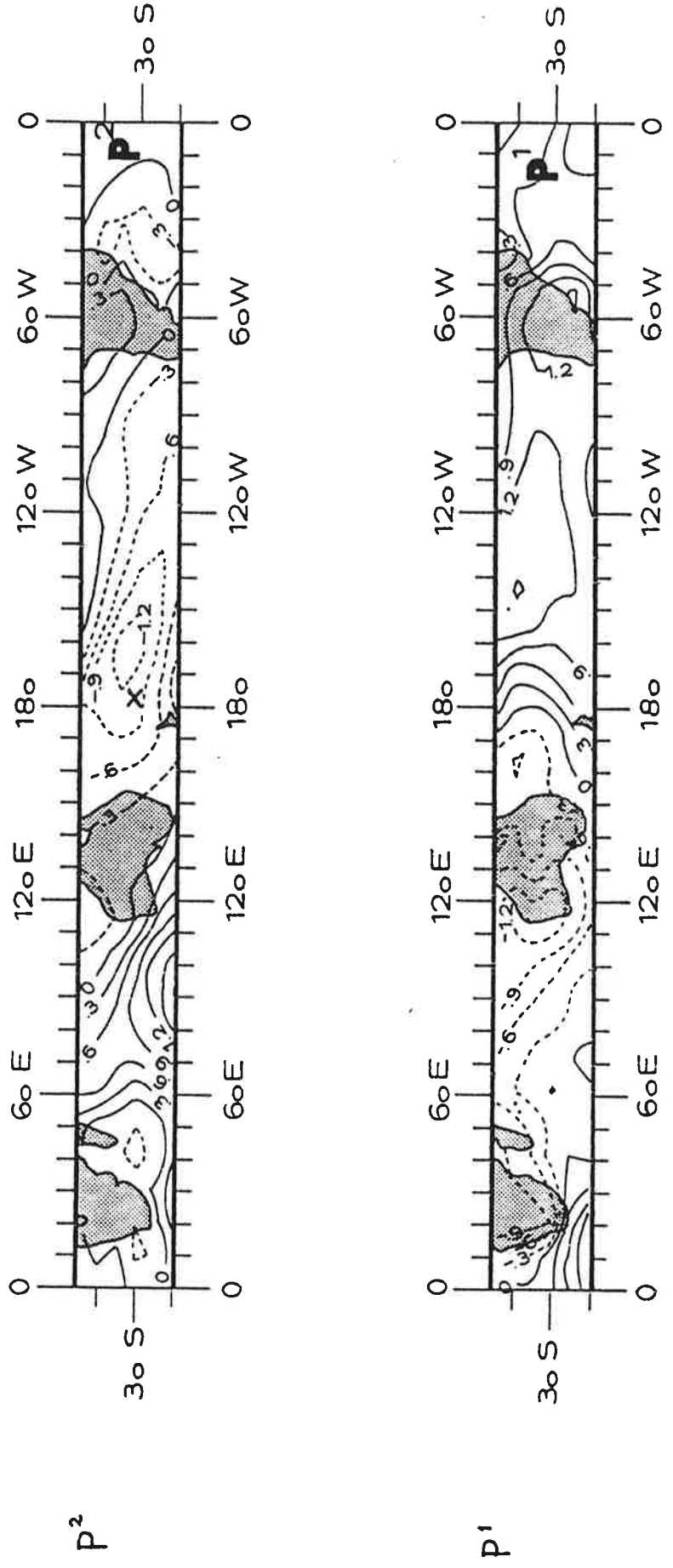

Figure 4:
POP patterns P^1 and P^2 of normalized Southern Hemisphere sea level pressure anomalies. The location of Raoul Island, used in Part V, is marked in P^2.

the Central and East Pacific and negative anomalies over Australia and the Indian Ocean, and these are connected with westerly wind anomalies in the eastern tropical Indian Ocean, easterly wind anomalies in the Pacific and northerly wind anomalies in the region near the dateline. According to the POP model and the oscillatory behavior described by $z^1(t)$ and $z^2(t)$, the pattern P^1 is gradually replaced by the pattern P^2 within a quarter of a rotation period, i.e., after about 7 to 9 months. This replacement appears in space as a smooth eastward migration of the negative P^1 anomaly into the western Pacific. The P^2 anomalies are connected with westerly wind anomalies over the tropical west Pacific. Half a period later the pattern $-P^1$ is dominant. It is associated with easterly anomalies over the eastern tropical Indian Ocean, westerly wind anomalies in the Pacific and southerly anomalies near the dateline. At three-quarters of a period ($-P^2$) there is a center of positive anomalies north of New Zealand, which is connected with easterly anomalies over the tropical west Pacific. After a full period the pattern P^1 reappears.

The results for the key variable reveals the description of the Southern Oscillation in a two-dimensional space as a linear damped oscillation. The temporal evolution of this oscillation is coherent with the traditional SOI. Differently from the SOI, the two-dimensional POP coefficient time series describes the timing of both the extreme phase and the onset phase of the Southern Oscillation. In space the oscillatory feature is characterized by eastward migration of pressure anomalies from the Indian Ocean into the central and east Pacific.

Questions to be asked now are:

- How does the signal appears in other variables, e.g. winds, SST, sea level?
- How much prediction skill is there in this two-dimensional space?
- What is the physical mechanism for the cyclic behavior described by the POPs?

These questions will be investigated in Parts III, IV and V.

PART III: GLOBAL FEATURES OF THE SOUTHERN OSCILLATION

The purpose of this part is to investigate the global features of the Southern Oscillation using the associated correlation pattern analysis. The SO- related variability in a certain parameter v is projected onto the two-dimensional space spanned by $\mathbf{P}^1$ and $\mathbf{P}^2$. The implicit assumption in doing so is that the SO - related variability in the variable v has the same oscillatory evolution as that described by z^1 and z^2. Two aspects are important:

- After the first verification using the SOI, it is also important to see whether the spatial evolution of anomalies described by the reduced system is consistent with more traditional studies, for instance the investigations of a particular event (Wyrtki, 1977, 1979) or classical composite analysis done by Rasmusson and Carpenter (1982) and by van Loon and his colleagues (van Loon and Madden, 1981; van Loon, 1984; van Loon and Shea, 1985; 1987). To make the comparison easier, the POP model is rotated in such a way that $z^1(t)$ has a maximum correlation with the SOI, and therefore $\mathbf{Q}_v$ ($-\mathbf{Q}_v$) describes the situation during a Cold (Warm) Event.
- In the two-dimensional system, the intervening state of the Southern Oscillation, i.e. $\mathbf{P}^2$, is well defined. Therefore the way of development from one extreme to the other is explicitly described. A systematic investigation of the intervening state as it appears in other variables might give a more complete picture of the Southern Oscillation.

7 DATA

All the data used in this part are unfiltered monthly anomalies. According to eq. (6) only time series in the period 51-58 and 72-88 are considered.

The Oceanic Data

Only surface data, the sea surface temperature (SST) and the surface topography, are available. The sea level data compiled by Wyrtki come from 41 stations located in the Pacific Ocean. The sea level time series extend from 1975 to 1988. The SST data have been analyzed by the National Meteorological Center (NMC). The data cover the area from 60°N to 40°S and extend from 1972 to 1988.

The sub-surface data, the ocean temperature and the zonal currents are available only as the output of a Oceanic General Circulation Model (OGCM) driven by the observed wind over decades (courtesy M. Latif). The OGCM described by Latif et al (1985) and Latif (1987) is a primitive equation model of the equatorial β-plane representing the tropical Pacific Ocean from 30°N to 30°S. The OGCM is quite capable of reproducing the interannual variations within the equatorial belt from 10°N to 10°S, especially along the equator (Latif, 1987). In the absence of observations from the real world, the modeled oceanic circulation is regarded as a substitute for real data in this study.

The Atmospheric Data

The global monthly mean SLP data for the period 1951 through June 1984 have been compiled by Barnett. The data extend from 42.5S to 72.5N. The results for the Northern Hemisphere SLP fields are similar to those using the Northern Hemisphere SLP analysis from the National Meteorological Center analysis.

The global wind field at 1000, 850, 500, 300 and 200mb, and the outgoing long wave radiation (OLR), were obtained from the National Meteorological Center Final Analysis for the period 1968-85. The data cover the area from 48°N to 48°S. The 1000 and 850-mb wind and the OLR data are only available from December 1975, December 1974 and June 1974 onwards respectively. The results of the low level wind data set are compared with those obtained from the surface wind data in COADS (Comprehensive Ocean Atmosphere Data Set).

Station data of air temperature and precipitation were extracted from the World Monthly Surface Station Climatology collected at the National Center of Atmospheric Research (NCAR). The data are available until 1987 in the form of monthly means for several hundred stations around the globe.

The monthly mean Northern Hemisphere 500 mb geopotential height analysis is obtained from the NMC analysis. The data are available from 20°N to 90°N for the period from March 1952 through December 1987.

The monthly mean Southern Hemisphere 500mb geopotential height are obtained from the Australian Bureau of Meteorology. The data cover the area from 10°S to 85°S and extend from 1972 to 1983.

The snow anomalies for the period from 1966 to 1987 are derived from weekly satellite snow cover observations compiled by the National Oceanic and Atmospheric Administration (NOAA). Anomalies are presented as deviations of the monthly snow cover frequency from the climatological monthly snow cover frequency.

8. THE TROPICAL OCEAN AND ATMOSPHERE

In the following sections the associated patterns Q_v^1 and Q_v^2 are calculated for the oceanic and atmospheric parameter v(t). According to equation (6), the evolution described by $Q_v^1 \rightarrow Q_v^2 \rightarrow -Q_v^1 \rightarrow -Q_v^2$ proceeds parallel to that identified by the POP analysis for the key variable, namely $P^1 \rightarrow P^2 \rightarrow -P^1 \rightarrow -P^2$. The relevance of this evolution in v to the cyclic evolution in the key variable is quantified by the explained variance.

8.1 THE TROPICAL OCEAN

Sea Surface Temperature (SST)

The associated SST pattern Q_{SST}^1 (Fig.5) shows the well known SST pattern of the Southern Oscillation extreme with strong negative SST anomalies in the tropical central and eastern Pacific, positive SST anomalies around Indonesia and negative SST anomalies in the Indian Ocean. Apart from the sign, this pattern is almost identical to Fig.1b in the Pacific and Indian Ocean. In Q_{SST}^2, SST anomalies are weaker than they are a quarter of the period earlier in Q_{SST}^1. Negative anomalies are found in the zonal belt between 5°N and 20°S in the central Pacific, with positive anomalies south and north of this belt. The variance of the unfiltered monthly mean SST anomalies explained by the associated patterns, Q_{SST}^1 and Q_{SST}^2, is above 40% in the central Pacific, and about 20% in the tropical Indian ocean.

Although there is a signal over the Indian Ocean, I will concentrate only on the variabilities in the Pacific because of the sparseness of data in the Indian Ocean.

Sea Level (SL)

The sea level variability in the Pacific ocean described by the POP model is shown in Fig.6. Note that the maps are derived from inhomogeneously distributed station data. Except for two islands and a few stations along the South American coast there are no data in the entire area 10°N-10°S, 170°E-90°W. The extreme phase of Southern Oscillation is characterized by the anomalous zonally orientated slope of sea level across the whole tropical

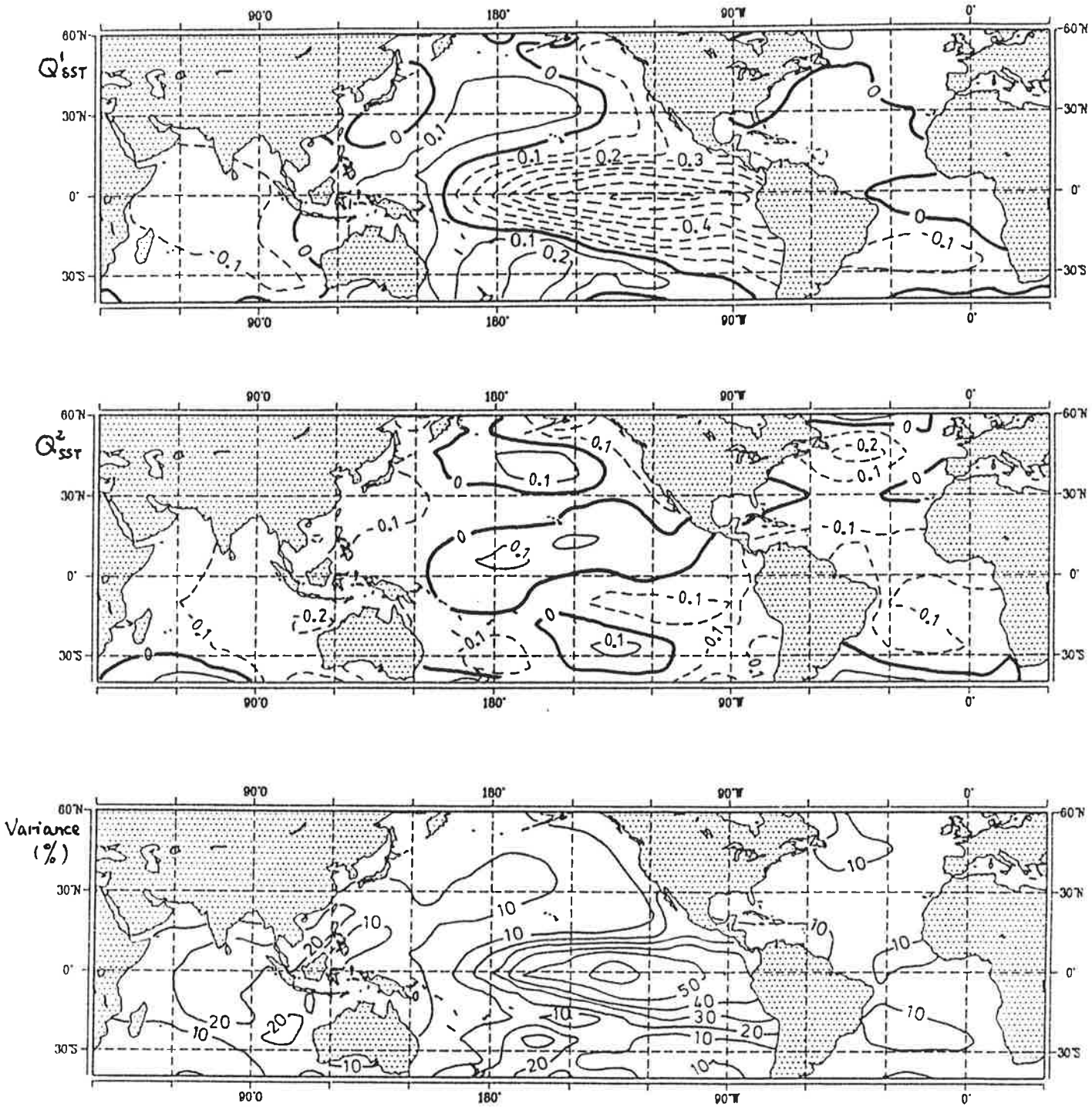

Figure 5:
Associated correlation patterns of sea surface temperature, Q^1_{SST} and Q^2_{SST}, and variance explained by these two patterns.. Units: ^oC

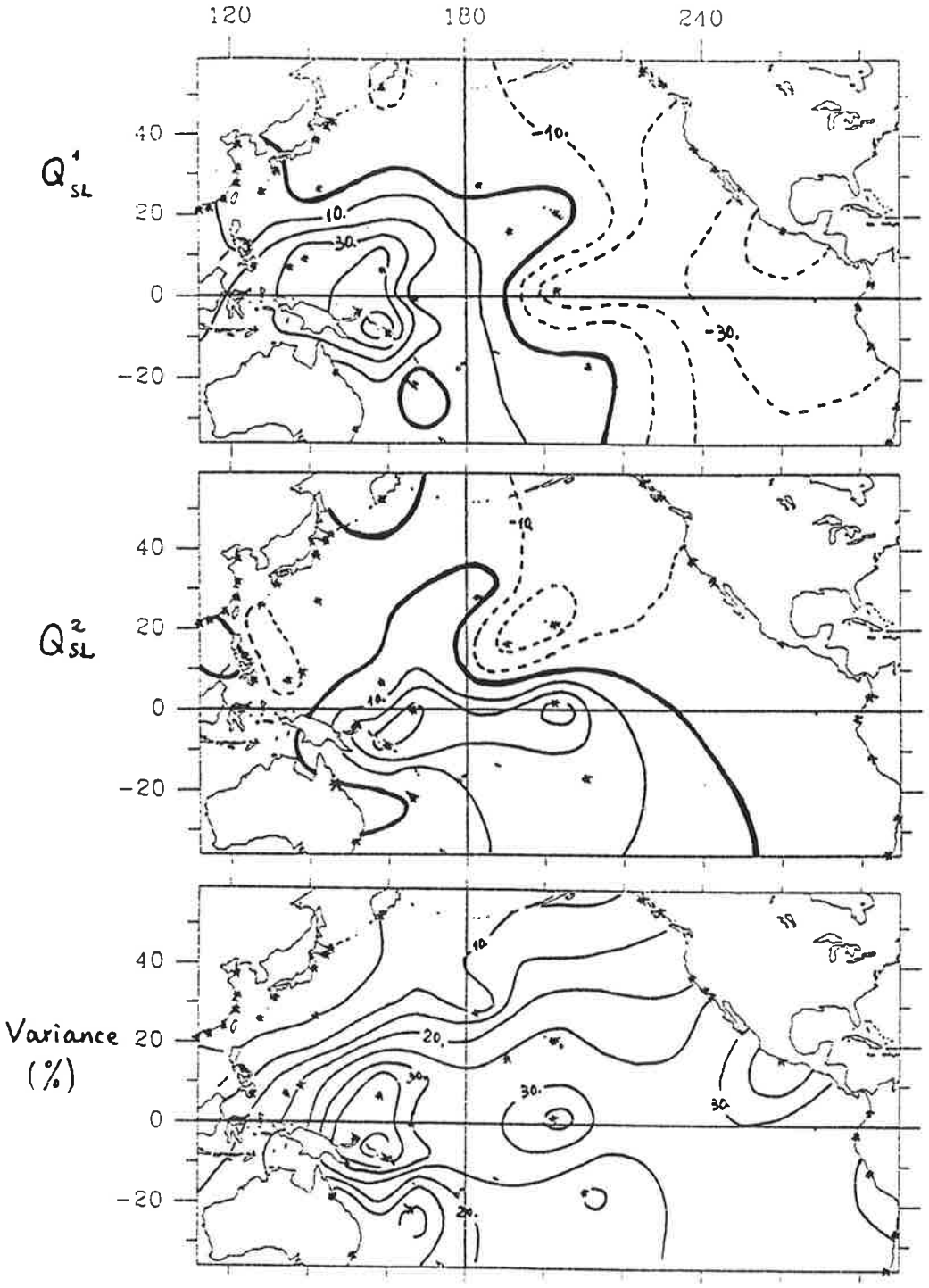

Figure 6:
Associated correlation patterns of sea level, Q^1_{SL} and Q^2_{SL}, and variance explained by these two patterns. The locations of the stations are marked by *. Units: mm.

Pacific Ocean. During a Cold Event (Q^1_{SL}) the sea level is tilted up, while during a Warm Event ($-Q^1_{SL}$) the sea level is tilted back against its normal slope. The intervening state (Q^2_{SL}) is described by large anomalies in the tropical west and central Pacific. In the framework of the POP model, namely $Q^1_{SL} \rightarrow Q^2_{SL} \rightarrow -Q^1_{SL} \rightarrow -Q^2_{SL}$, the tropical sea level variability appears as an eastward movement of the positive sea level anomalies from the Indonesian region (Q^1_{SL}) to the western and central Pacific (Q^2_{SL}) and finally to the eastern Pacific ($-Q^1_{SL}$). In the sub-tropical Northern Hemisphere the negative sea level anomalies seem to propagate from the eastern Pacific (Q^1_{SL}) to the central Pacific (Q^2_{SL}) and to the western Pacific ($-Q^1_{SL}$). This westward migration in the subtropics has much smaller amplitude and is less well defined than the tropical eastward migration. The variance explained by Q^1_{SL} and Q^2_{SL} is about 30-35% in the tropical region and about 20% in the subtropics.

The anomalous topography in Fig.6 should relate to the anomalous geostrophic current. In Q^1_{SL}, $\frac{1}{f}\frac{\partial p}{\partial y}$ is positive in most of the ocean, indicated by lower sea level along the equator than at 20°S and 20°N. This feature is associated with the anomalous tropical westward current, i.e., the South Equatorial Current (SEC) is stronger and the North Equatorial Counter Current (NECC) is weaker than normal. In Q^2_{SL} however, $\frac{1}{f}\frac{\partial p}{\partial y}$ is negative in the west and central Pacific with higher sea level in the tropics than in the regions south and north of it. It means that in the intervening state before a Warm event, an anomalous current flows eastward in the west and central Pacific.

The sea level related current anomalies in the extreme phase of the SO, i.e. stronger SEC and weaker NECC, were also described by Wyrtki (1977, 1979) and substantiated by numerical integrations (Philander and Seigel, 1985; and Latif, 1987).

Sub-Surface Temperature (ST)

The associated correlation patterns for the (model - generated) ocean temperature in the vertical section along the equator are demonstrated in Fig.7. During the cold event (Q^1_{ST}) negative temperature anomalies are found all along the equator at the surface, and also in the east Pacific at the deeper layer. In the west Pacific positive temperature anomalies appear at 200-m depth. These positive temperature anomalies, which are consistently

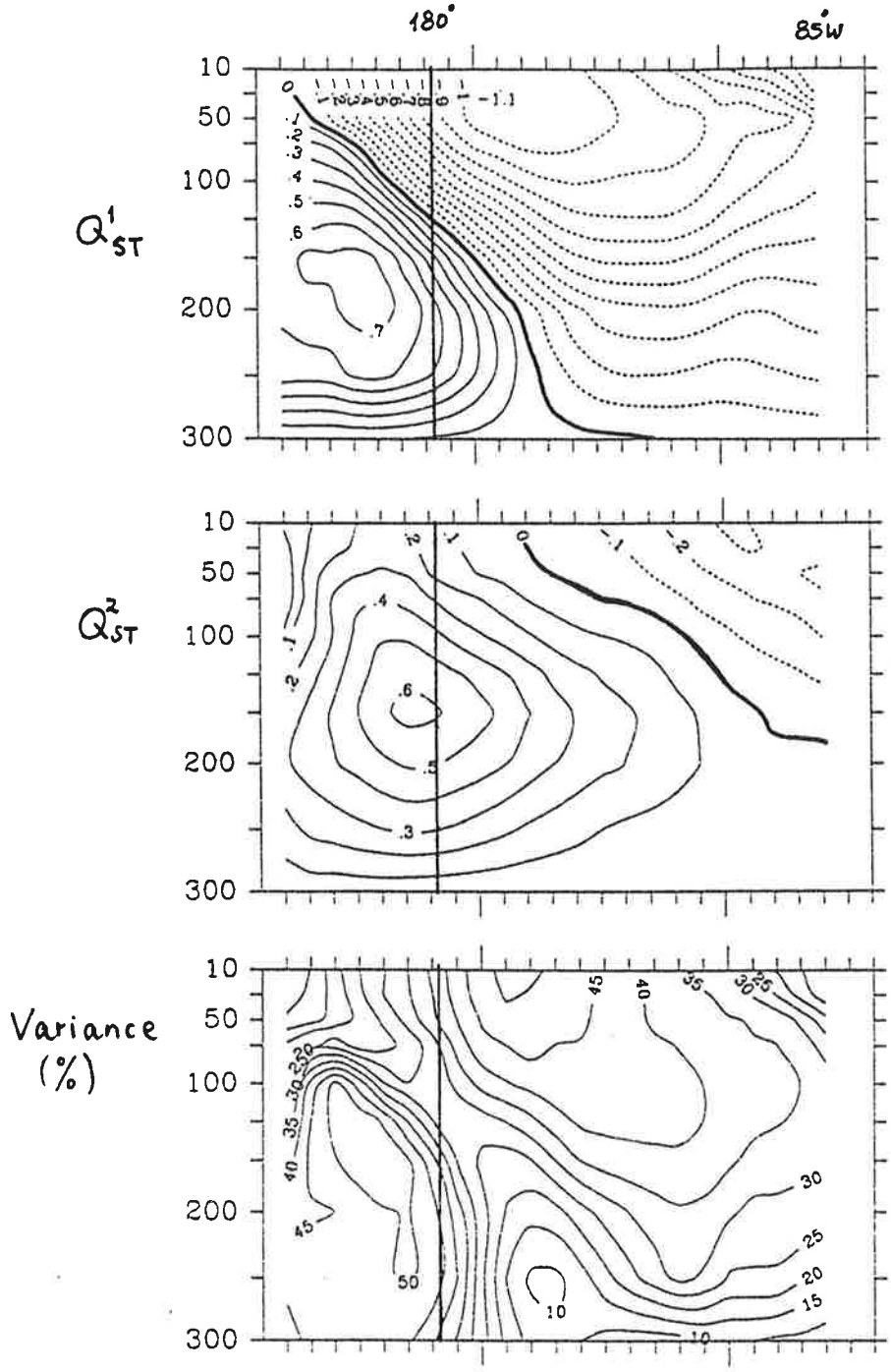

Figure 7:
Associated correlation patterns of the simulated sub-surface temperature Q^1_{ST} and Q^2_{ST} in the vertical section along the equator. Units: ^oC

associated with above normal sea level (Q^1_{SL}), represent a deepened thermocline and thus a surplus of warm water in the west Pacific. In the onset phase of a Warm Event (Q^2_{ST}) this pool of anomalous warm water has expanded upward and eastward and occupies a large part of the equatorial ocean with maximum values located near the dateline at 150-m depth. The explained variance is large and about 50% in the central/eastern and the western part of the equatorial Pacific.

The Surface and Sub-surface Zonal Currents (ZC)

The associated correlation patterns for the simulated zonal current anomalies in the vertical section along the equator are shown in Fig.8. In the cold phase of the Southern Oscillation (Q^1_{ZC}) the anomalous surface current flows westward across the entire equator, i.e., the South Equatorial Current is stronger than normal, whereas the sub-surface state is characterized by intensified (eastward) Equatorial Undercurrent (EUC). The SEC is confined to the first 50 meters, with maximum values at the surface, and the anomalous undercurrent expands through 300-m depth with maximum values near 100-m. In the intervening state Q^2_{ZC} the surface current has an anomalous eastward component in the west and central Pacific, but the undercurrent remains stronger than normal except for the most western part of the ocean where the undercurrent is weaker than normal. The variances explained by these patterns are about 50% in the central ocean. Larger explained variances of about 20% are also found in the west Pacific in 100 to 150-m depth and in the central Pacific at the surface.

The geostrophic relationship is no longer valid in the equatorial region. The Equatorial Undercurrent is driven by the pressure force, while the South Equatorial Current is forced directly by surface winds. The relationship between oceanic circulation and atmospheric forcing will be discussed later.

Summary: the SO - related Features in the Tropical Pacific

In Fig.9 the SO signal in the tropical Pacific Ocean is reduced in a two-dimensional space spanned by two idealized patterns Q^1_0 and Q^2_0, in which the anomalous sea level and zonal current changes are taken from the associated correlation pattern shown above, and the anomalous thermocline

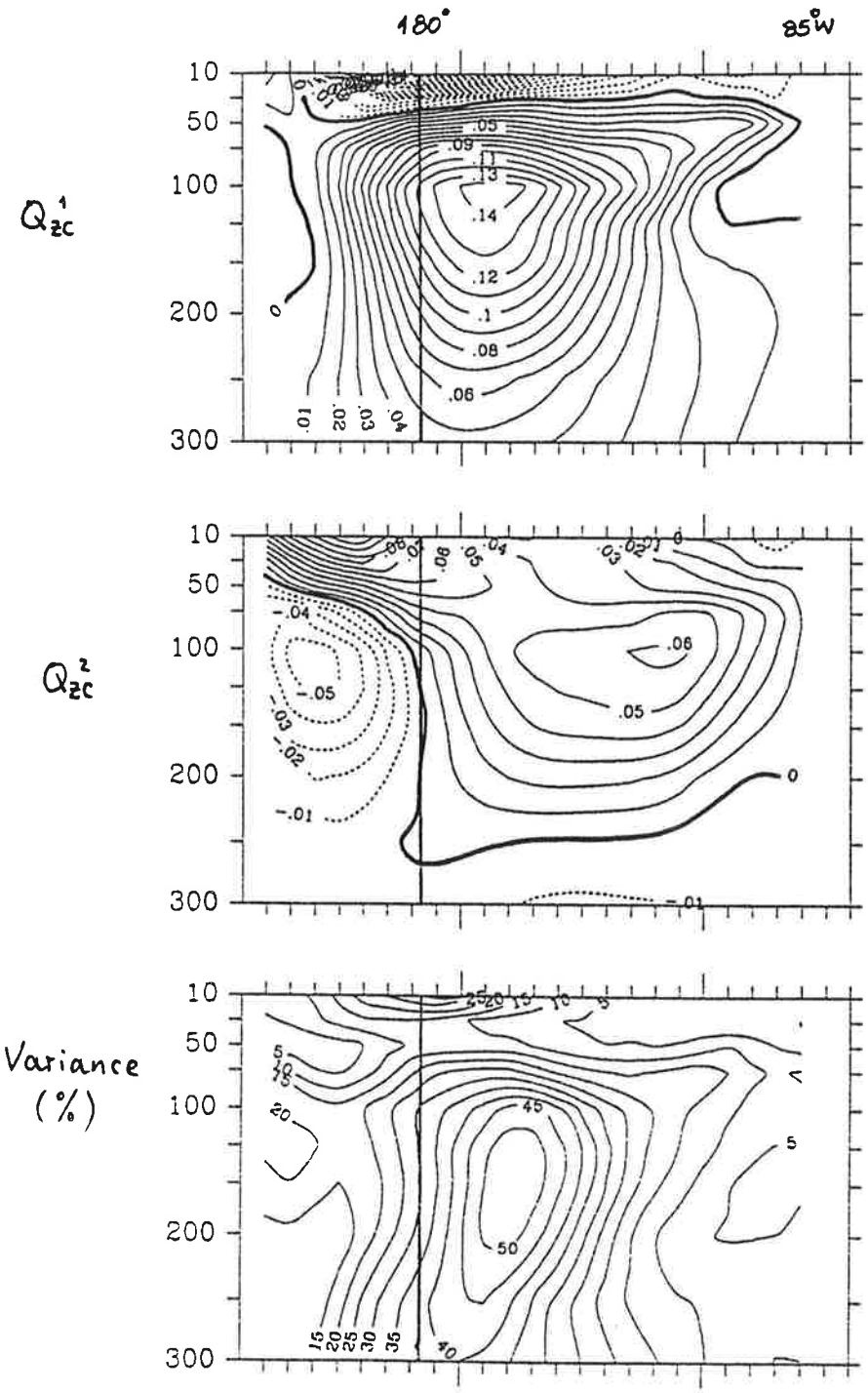

Figure 8:
Associated correlation patterns of the simulated surface and sub-surface zonal current Q^1_{ZC} and Q^2_{ZC} in the vertical section along the equator, and variance explained by these two patterns. Units: cm/s

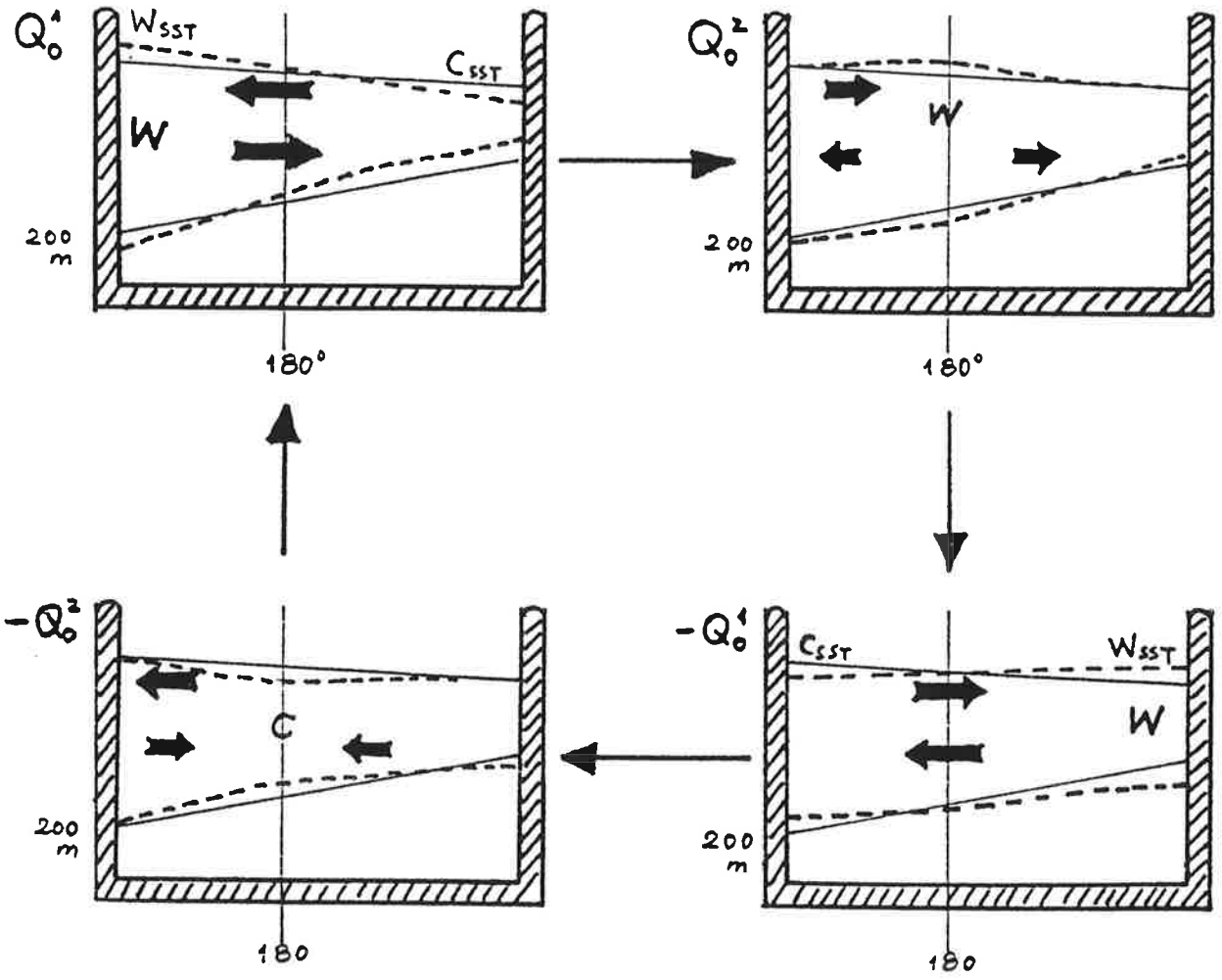

Figure 9:

Schematic diagram of the the SO-related behavior in the equatorial Pacific ocean. The thin lines describe the normal slope of the sea level and the thermocline. The heavy dashed lines represent the anomalous position of the sea level and the thermocline. The arrows show the surface and the sub-surface zonal current anomalies. The letters 'W' ('W_{SST}') and 'C' ('C_{SST}') mark the regions with anomalously warm and cold water in the upper layer (at the sea surface) respectively.

changes are interpolated from the temperature anomalies in the sub-surface. Fig.9 shows that the occurrence of the positive (negative) SST anomalies in the east Pacific appears as a logical consequence of the oscillatory development of physically meaningful patterns.

Before a Warm Event (Q_0^1 in Fig.9), the slope of the sea level and of the thermocline, and the westward surface current and the eastward under current are stronger than normal. The lifted sea level and deepened thermocline reflect the presence of a warm water excess in the subsurface of the western Pacific. Positive sea surface temperature anomalies are also evident in the west Pacific at this stage. After a quarter of a period in the intervening state Q_0^2, anomalous eastward surface current west of the dateline and horizontally subsurface divergent flow (at about 100 meter) in the central Pacific are found. At the same time sea level has risen and the thermocline has been lowered in the central Pacific, i.e., anomalous downwelling, or a reduction of the mean upwelling, is taking place. The reduction of the upwelling and the eastward advection (by means of an anomalous surface current) of the west Pacific warm water lead to the positive temperature anomalies in the central Pacific. However the positive temperature anomalies are concentrated at about 150-m depth. It means that no considerable temperature anomalies appear at the surface in the intervening stage. During a Warm Event ($-Q_0^1$), the warm water is located in the eastern Pacific, the anomalous surface and sub-surface currents flow in the opposite direction from those of half a period earlier, the sea level and thermocline tilt back against their normal slope. The evolution before and at a Cold Event is the opposite of that just described.

It is concluded that the extreme warm (cold) phase of Southern Oscillation takes place after the building up of an excess of warm (cold) water in the upper layer of the west Pacific and an upward and eastward migration of part of the warm (cold) water into the central and east Pacific. This migration of anomalies is due partly to the reduced (intensified) upwelling and partly to the eastward advection of temperature anomalies via the anomalous surface current.

This result is consistent with the observations from Wyrtki (1985). However, the cyclic evolution, its different stages of the action chain, and the

associated equatorial circulation anomalies, are presented more completely by the POP analysis.

8.2. TROPICAL ATMOSPHERE

In this section the associated correlation patterns and variance explained by these patterns are presented for atmospheric parameters. Compared with the results in the previous section, the portion of variance connected with the SO is generally smaller in the atmosphere than in the ocean. This is certainly due to the fact that the atmosphere is much more energetic than the ocean in the high frequency band, partly due to the tropical 30- to 60- day oscillations (the explained variance is calculated for the unfiltered data).

Sea Level Pressure (SLP)

Because of the rotation, as mentioned at the beginning of part III, the associated correlation patterns are slightly different from the POPs in the Southern Hemisphere subtropics. In the tropics, Q^1_{SLP} (Fig.10) reveals the familiar Southern Oscillation signal in its cold phase with negative anomalies over South Africa, the Indian Ocean and the Indonesian region, and the positive anomalies over the central and east Pacific. In the intervening stage (Q^2_{SLP}), the dominant tropical features are the two well developed cyclonic pressure anomalies straddling the equator in the west and central Pacific. An eastward migration of the negative pressure anomalies from Africa and the Indian Ocean in Q^1_{SLP} into the subtropical west and central Pacific in both hemispheres in Q^2_{SLP} is obvious. The explained variance (Fig.10) is largest over the area south of 20°N with maximum values of about 20% over the region of the Southern Hemisphere subtropical high. Similar patterns are obtained from the canonical correlation analysis (Graham et al., 1987) and from the composites analysis (van Loon and Shea, 1985).

Winds at 850 and 200-mb (W8 and W2)

The low level winds (winds at 1000-mb, 850-mb and 700-mb) wind patterns are almost identical, and geostrophically consistent with the pressure patterns Q^1_{SLP} and Q^2_{SLP}. Also the wind patterns at 300-mb and 200-mb are similar. In

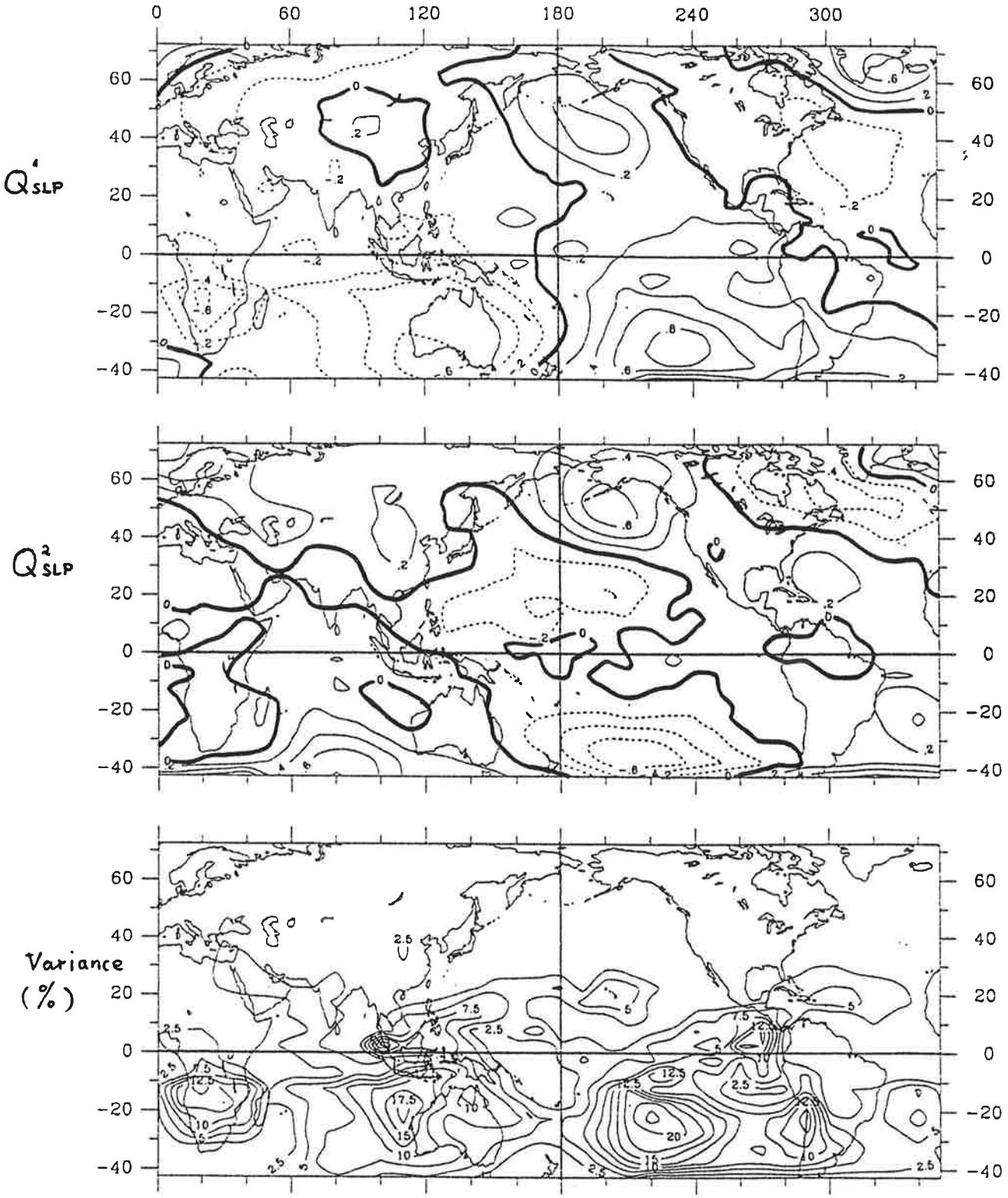

Figure 10:
Associated correlation patterns of global sea level pressure anomalies, Q^1_{SLP} and Q^2_{SLP}, and variance explained by these two patterns. Units: mb.

contrast to the low and upper level winds the signal at 500-mb is very weak and patchy (not shown). I will therefore concentrate only on the winds at 850-mb, as representative of the low levels, and those at 200-mb for the upper levels. In Fig. 11 and 12 the associated correlation patterns and the variance explained by the zonal and meridional winds are presented for the 850-mb and 200-mb levels respectively.

In the cold phase of the SO, the tropical 850-mb wind pattern (Q^1_{W8} in Fig.11) shows westerly wind anomalies over the Indian Ocean, easterly wind anomalies over the central Pacific and westerly wind anomalies over the northern part of the South America and the west Atlantic. On the other hand, at 200-mb (Q^1_{W2} in Fig.12) anomalies with opposite sign are found. These large scale wind patterns indicate zonally orientated cell structures with low level convergent motions over the Indonesian region and low level divergent motions over the east Pacific in the entire tropical troposphere. According to the POP concept, a Warm Event is characterized by $-Q^1_{W8}$ and $-Q^1_{W2}$, i.e. low level divergent motions over the Indonesian region and low level convergent motions over the east Pacific. These two anomalous circulations describe the variations of the directly thermally driven Walker Circulation, which is understood as the atmospheric response to the warm SST distribution. Mass flows usually into the warm water region at low level, picks up water vapor on its way, rises over the warmest water to the top of the troposphere with the help of released latent heat, diverges at the upper level, and eventually sinks over the region with colder SST. During a Cold Event, an extra amount of warm water is situated in the Indonesian region (Q^1_{SST} in Fig.5), whereas during a Warm Event, the warm water is displaced eastward over the central and east Pacific ($-Q^1_{SST}$). Associated with these two extremes of SST distribution, the ascending branch of the Walker Circulation is located over the Indonesian region in a Cold Event (Q^1_{W8}, Q^1_{W2}), and over the central and east Pacific in a Warm Event ($-Q^1_{W8}$, $-Q^1_{W2}$), a result which has been obtained also by many other authors (e.g. Rasmusson and Carpenter, 1982).

Another feature of the 200-mb wind in Q^1_{W2} ($-Q^1_{W2}$) is the two cyclonic (anticyclonic) cells straddling the equator. This is consistent with the observations (e.g. in 1982/83) and the result of the simplified theory (Gill, 1980) and other numerical studies (e.g., Shukla and Wallace, 1983) that an equatorial upward motion (forced by positive SST anomalies) is associated with

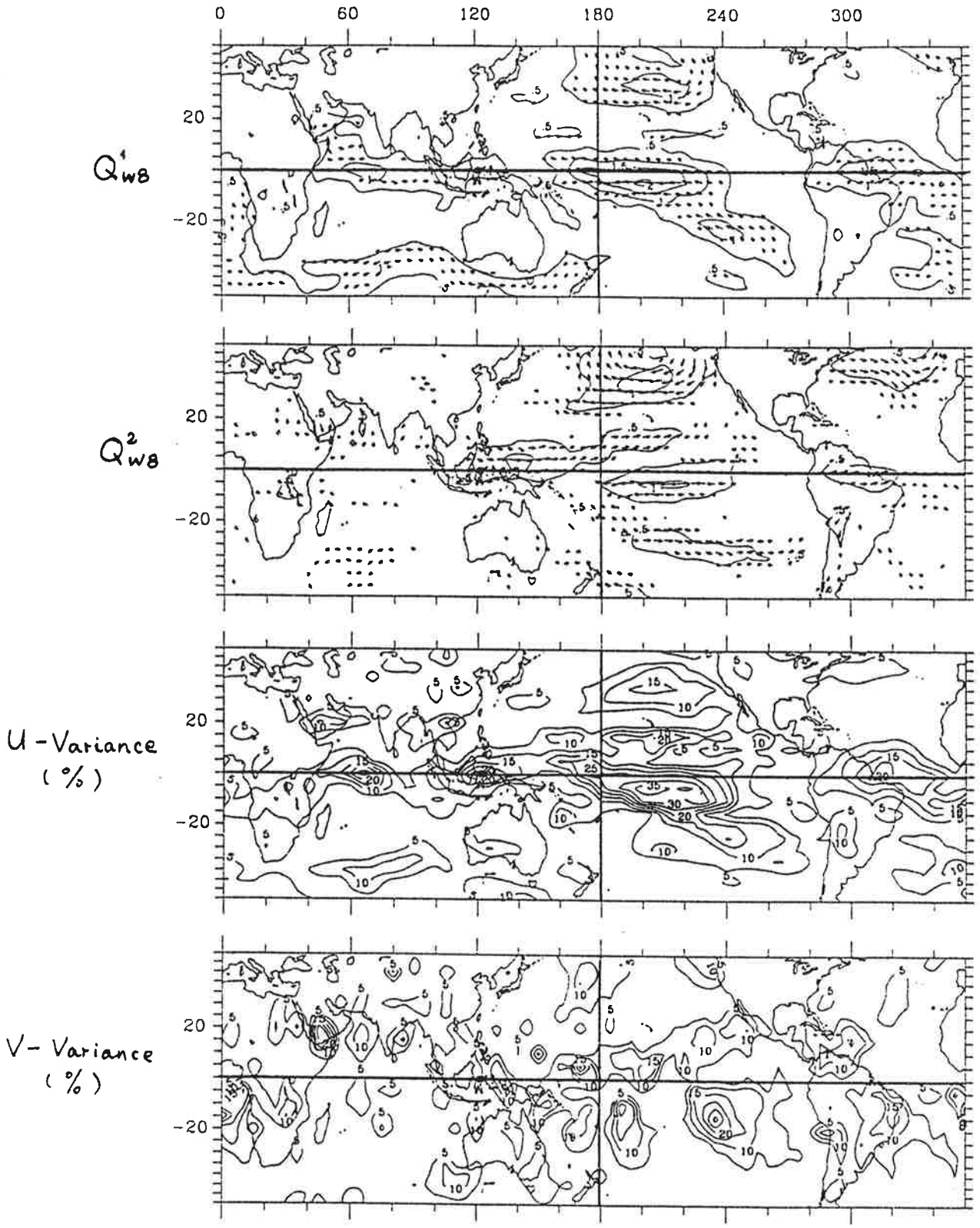

Figure 11:
Associated correlation patterns of 850-mb wind anomalies, Q^1_{WS} and Q^2_{WS}, and variance explained by the zonal and meridional components of these two patterns.

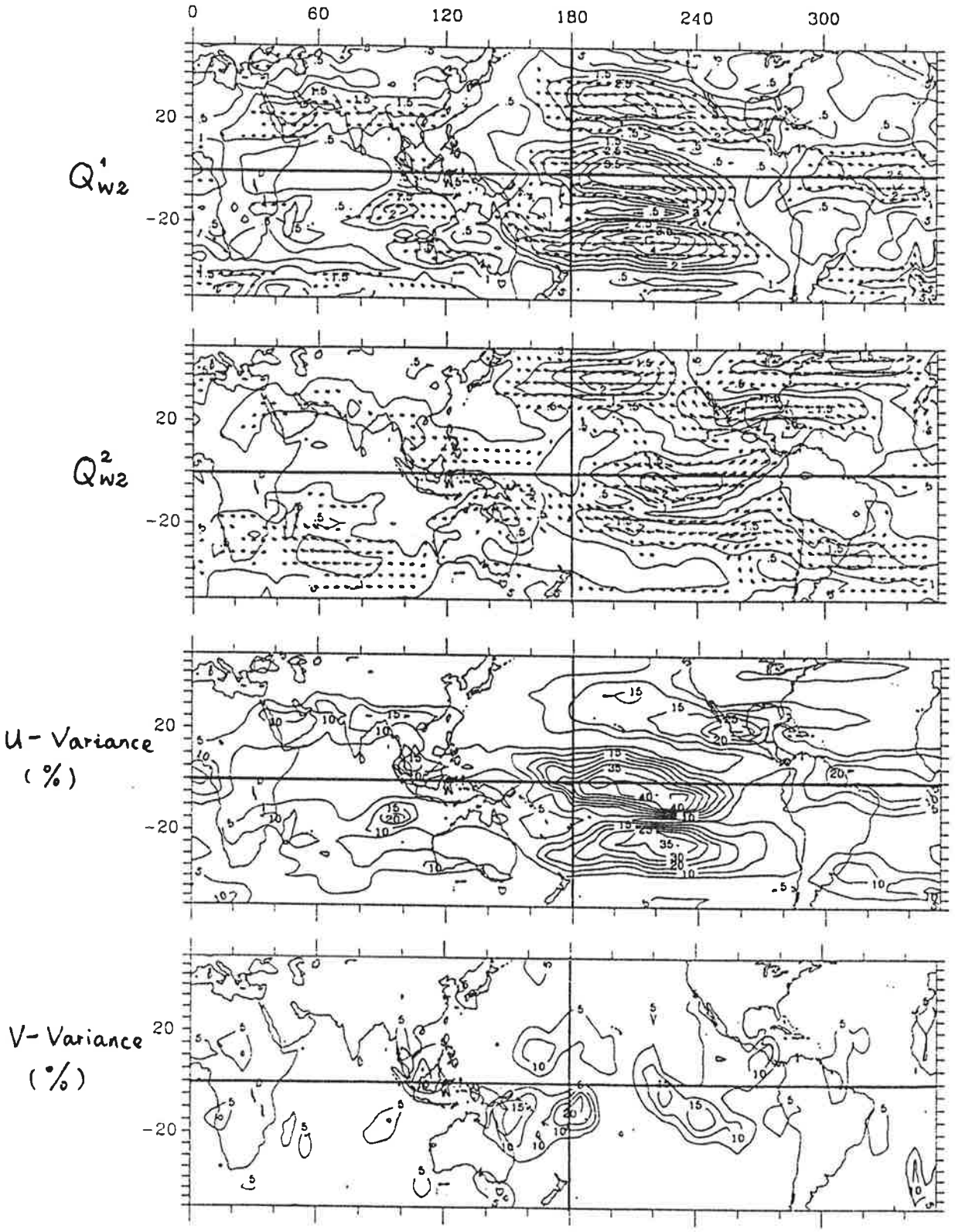

Figure 12:
Associated correlation patterns of 200-mb wind anomalies, Q^1_{W2} and Q^2_{W2}, and variance explained by the zonal and meridional components of these two patterns.

anomalous divergent outflow and two anomalous anticyclones at the upper level.

At the intervening stage, the low level convergence in the region just west of the dateline and the low level divergence over the central Pacific (Q^2_{W8}) are found. At 200-mb (Q^2_{W2}) anomalies of opposite sign appear, i.e. there is divergent motion over the west Pacific and convergent motion over the east Pacific. It means that the zonal displacements of the ascending branch of the Walker Circulation described by Q^1_{W8}/Q^1_{W2} and $-Q^1_{W8}/-Q^1_{W2}$ happen quite slowly: there is an eastward migration from the Indonesian region (in Q^1_{W8} and Q^1_{W2}) into the west Pacific region (in Q^2_{W8} and Q^2_{W2}) and into the central and east Pacific (in $-Q^1_{W8}$ and $-Q^1_{W2}$). The wind variance explained by the variation of Walker circulation (the zonal wind component; Fig.12c) is about 20 to 40% in the tropics.

The mean SST distribution has not only the large scale zonal asymmetries which are responsible for the Walker Circulation, but also meridional asymmetries. Generally, the warmest water is located north of the equator in the east Pacific, and north and south of the equator in the west Pacific, while a cold water tongue occupies the equatorial central and east Pacific. Corresponding to this SST distribution, convective motions are observed over the south west Pacific (South Pacific Convergence Zone (SPCZ)) and north of the equator (Intertropical Convergence Zone (ITCZ)). During a Warm Event, an excess of warm surface water is situated in the equatorial central and east Pacific ($-Q^1_{SST}$), i.e. the cold water tongue in the equatorial central and east Pacific is weakened. Consequently, the SPCZ and ITCZ both move equatorward during a Warm Event. This feature has been identified by many other observational studies (e.g. Rasmusson and Carpenter, 1982, Kiladis and van Loon, 1988).

However, as shown in Fig.11 and 12, the anomalous v-wind has much smaller amplitude than than that of the anomalous u-wind. Also the variance explained by v-winds (5-10%, Fig.11d and Fig.12d) is smaller than that explained by u-winds (15-30%, Fig.11c and Fig.12c). Therefore, to extract a clear signal in the meridional wind field, the associated correlation patterns for the v-winds are averaged over the central Pacific (160°E-160°W) and shown in a latitude-height section in Fig.13 (Q^1_V and Q^2_V).

Consistent with other investigations, the associated pattern for the cold

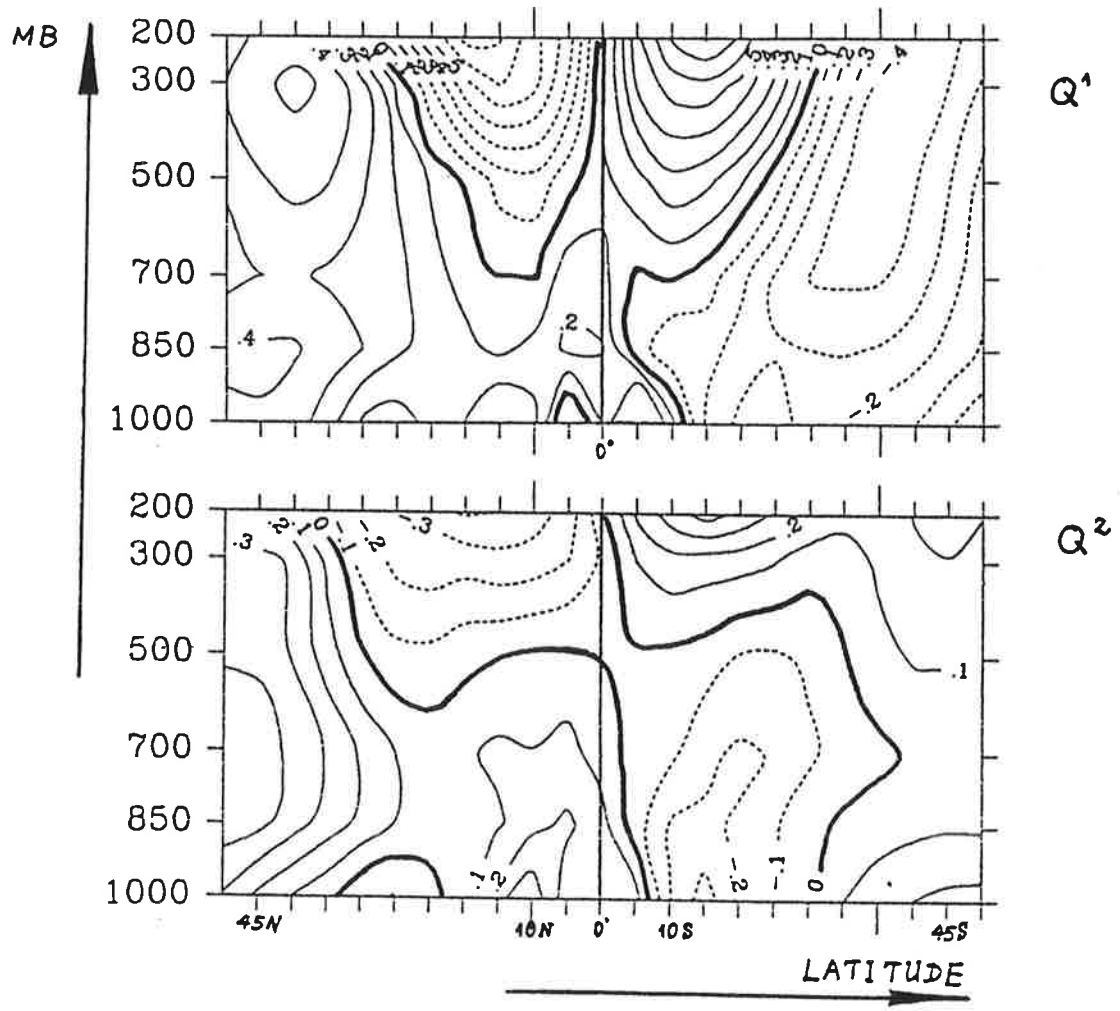

Figure 13:
Latitude-height section of the zonally averaged (160°E-160°W) associated correlation patterns of the v-winds.

(warm) phase Q_V^1 ($-Q_V^1$) shows low level northerly (southerly) wind anomalies south of the equator and low level southerly (northerly) wind anomalies north of the equator, indicating a poleward (equatorward) movement of both the SPCZ and the ITCZ, and anomalous divergent (convergent) motion; at upper levels the opposite situation is found, indicating convergent (divergent) motion. This pattern describes the variation of the meridionally orientated Hadley Circulation, namely an intensification of the circulation during the warm phase and a weakening of the circulation during the cold phase of the SO. In the intervening state (Q_V^2), the baroclinic structure also exists in the tropical troposphere. At upper levels the anomalies are weaker than a quarter of a period earlier, but at low levels southerly wind anomalies are well developed in the Southern Hemisphere subtropics, and low level northerly wind anomalies appear in the tropics with largest values around 10°-15°N.

The Outgoing Long Wave Radiation (OLR)

Anomalies of the tropical OLR are a good approximation of anomalous tropical rainfall and convection (Arkin, 1982). The energy connected with convective motion is the latent heat that is released when the moist air rises. If more latent energy is released, then the cumulus clouds are higher, and their top surface temperatures are lower, i.e. the OLR has negative anomalies. Therefore OLR anomalies vary linearly with anomalies of the divergent flow as long as the total low level flow is convergent.

The dominant feature in Fig.14 is the eastward shift of the convective area with negative OLR anomalies near 125°E and positive OLR anomalies near 170°W in Q_{OLR}^1, and negative OLR anomalies near 155°E and positive OLR anomalies near 150°W in Q_{OLR}^2. It is consistent with the eastward migration of the ascending branch of the Walker Circulation. The variance explained by the SO-related OLR variability is about 20-40% over the tropical Pacific.

Summary: the SO - Related Features in the Tropical Pacific

From the presented results, it is concluded that in the tropical atmosphere the SO-related signal is stronger in the zonally orientated circulation (explained variance of about 15-30%) than in the meridionally orientated circulation (explained variance of about 5-10%), i.e. the large scale mass

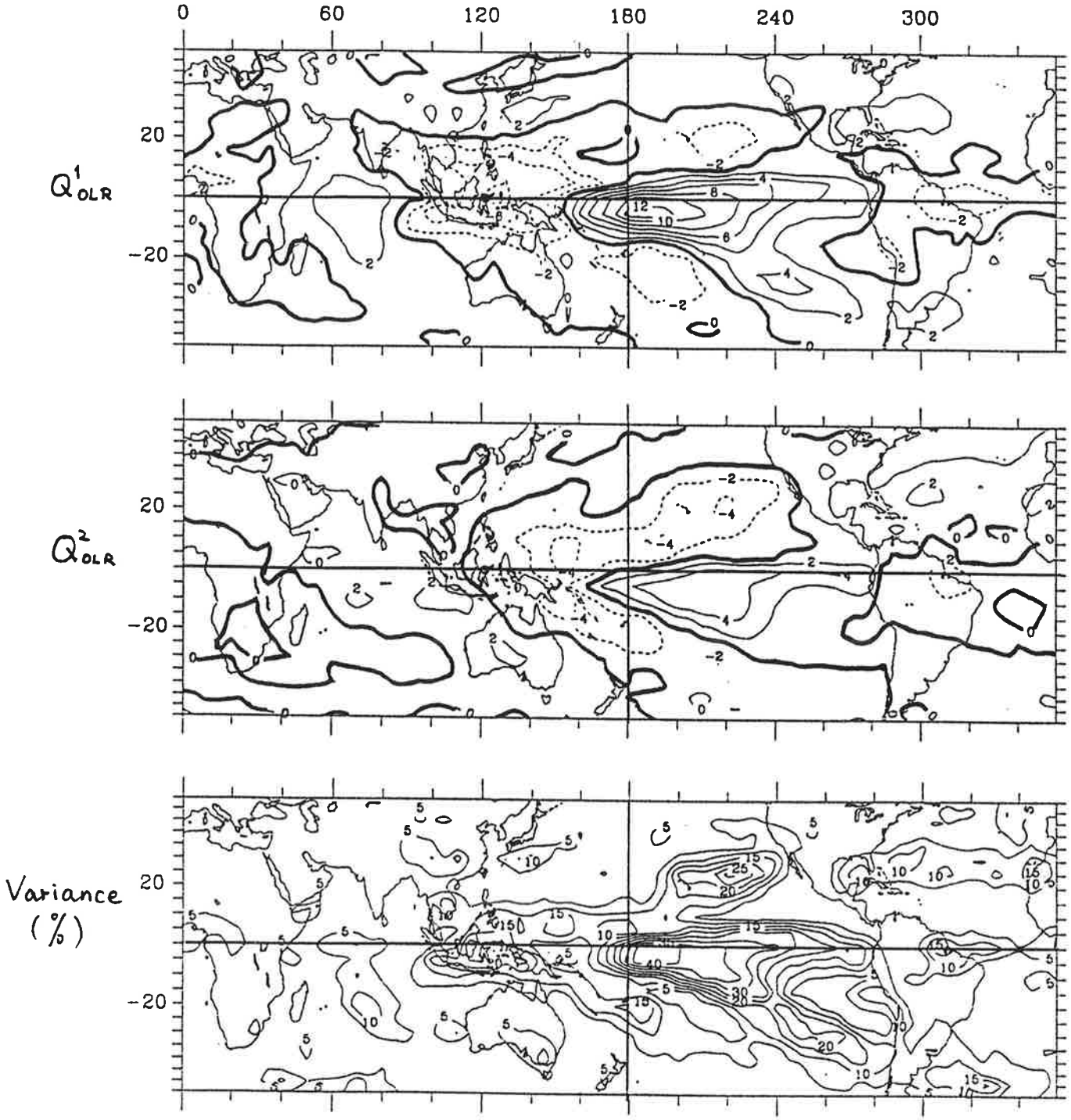

Figure 14:
Associated correlation patterns of outgoing long wave radiation anomalies, Q^1_{OLR} and Q^2_{OLR}, and variance explained by these two patterns.

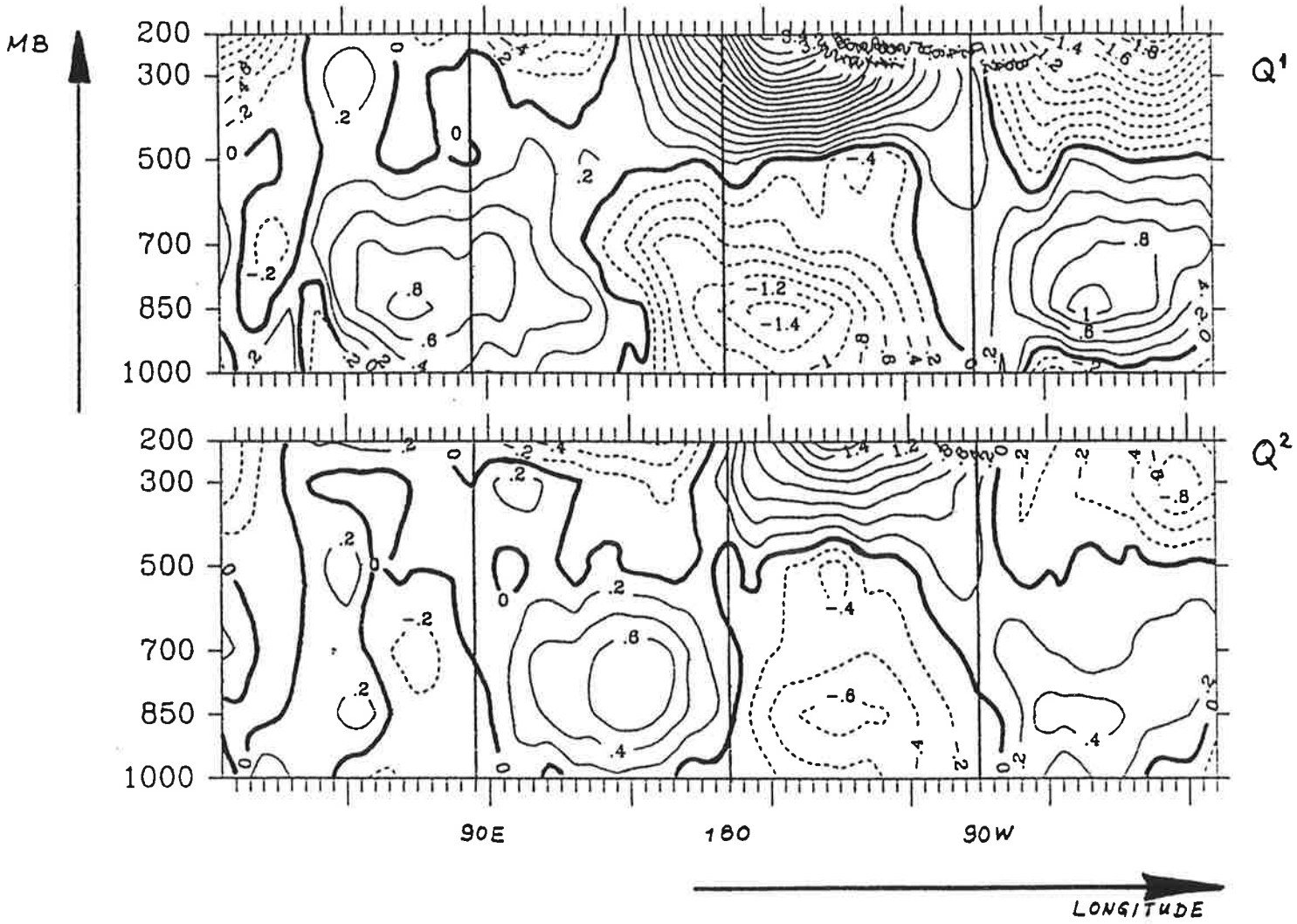

Figure 15:
Longitude-height section of the meridionally averaged (5°S-5°N) associated correlation patterns of the u-winds.

displacement is connected mainly with variations of the zonal circulation.

These variations are summarized in Q_U^1 and Q_U^2 (Fig.15), which show the meridionally averaged ($5^\circ S$-$5^\circ N$) associated correlation patterns for the zonal wind at different levels. Well - defined cell structures are found in Q_U^1 and Q_U^2. The warm phase of the SO appears as a logical consequence of the oscillatory development of patterns Q_U^1 and Q_U^2. The development is characterized by an eastward migration of the cell structure, which is connected with low level westerly wind anomalies, from the Indian ocean region (in Q_U^1) into the west Pacific (in Q_U^2), and finally into the central Pacific (in $-Q_U^1$).

The eastward propagation of anomalous winds was also found by Gutzler and Harrison (1987), and is consistent with the evolution of OLR anomalies. However, this eastward propagation is not uniform. The entire process shows its largest strength during the warm and cold phases of the SO.

9 OTHER ATMOSPHERIC PARAMETERS

Extratropical Northern Hemisphere

The 500-mb geopotential height anomalies in the cold phase (Q^1_{N5Z}) and the onset phase of a Warm Event (Q^2_{N5Z}) (Fig.16) are similar and dominated by a chain of centers of action with positive anomalies over the north Pacific, negative anomalies over the north part of North America, positive anomalies over Greenland, and finally a negative anomaly center over north Europe. The variance explained by Q^1_{N5Z} and Q^2_{N5Z} in the extratropics is much smaller than in the tropics, but shows relative large values near the action centers described above.

Similar patterns are found for the SLP field (Fig.10). This indicates that the SO-related signal is barotropic in the Northern Hemisphere extratropics.

The wind anomalies are geostrophically consistent with pressure patterns. However, the largest anomalies appear only over the north Pacific near 35°N-40°N (at least in the analysis domain 48°N-48°S). During the cold phase and the onset phase, anticyclonic wind anomalies with strong easterlies at its southern branch are found in both the low and upper levels (Fig.11 and 12).

This large scale barotropic feature is demonstrated more clearly in Fig.17, where associated correlation patterns for zonal wind anomalies are averaged in the area between 33°N and 41°N and plotted in a longitude-height section. During the half cycle ($Q^1 \rightarrow Q^2$), easterly anomalies appear over the Pacific in the entire troposphere. West and east of this region westerly anomalies are found with much smaller amplitude and again in the entire troposphere.

Extratropical Southern Hemisphere

The associated correlation patterns for the Southern Hemisphere 500-mb geopotential height are shown in Fig.18 (Q^1_{S5Z} and Q^2_{S5Z}). During the cold phase and onset phase of the SO, positive anomalies are found in the mid-latitudes and negative anomalies in the high latitudes. Similar patterns are found for the SLP field south of 45°S (not shown). Again in the mid- and high latitudes

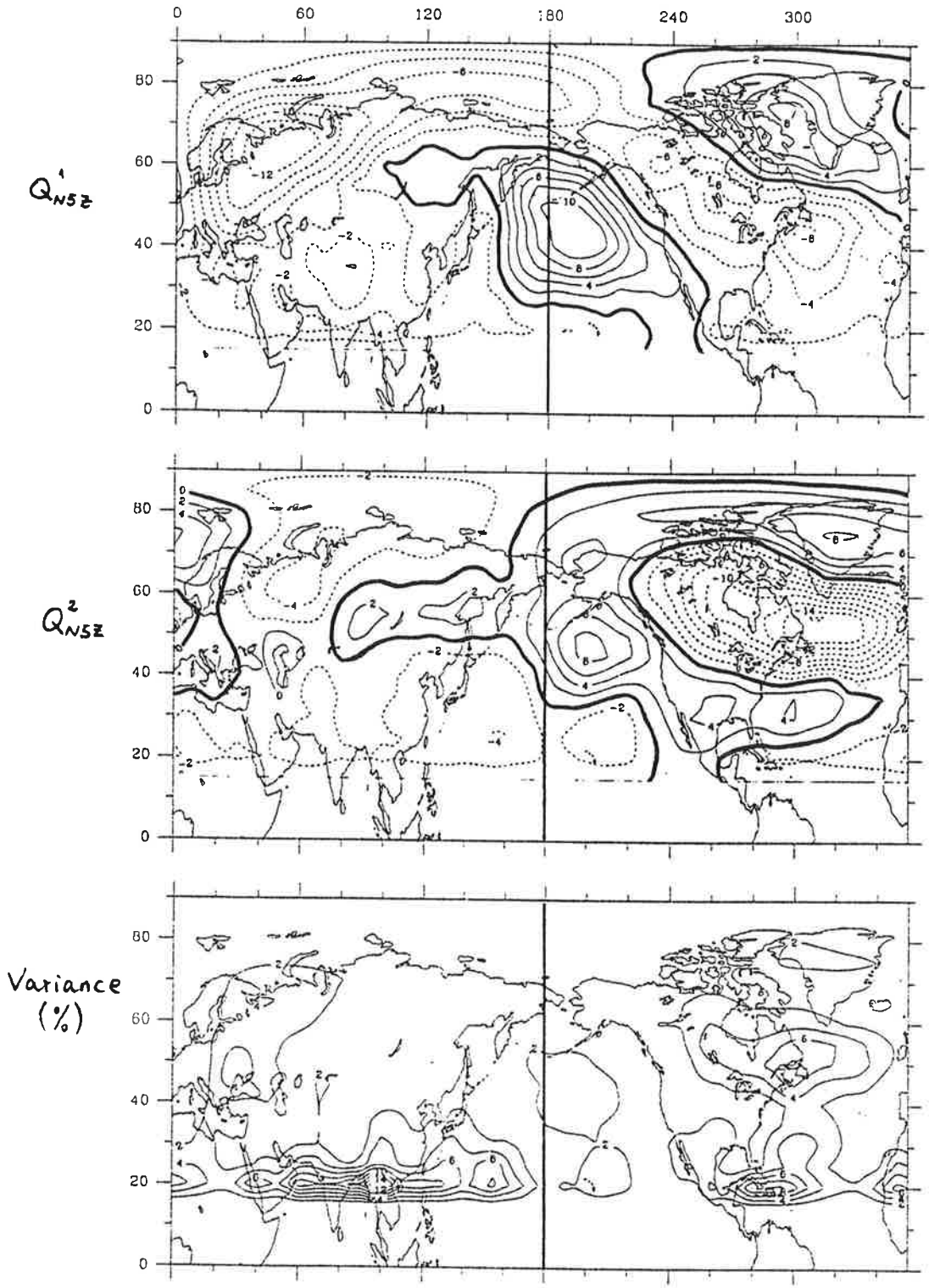

Figure 16:
Associated correlation patterns of Northern Hemisphere 500-mb geopotential height anomalies, Q^1_{NSZ} and Q^2_{NSZ}, and variance explained by these two patterns.

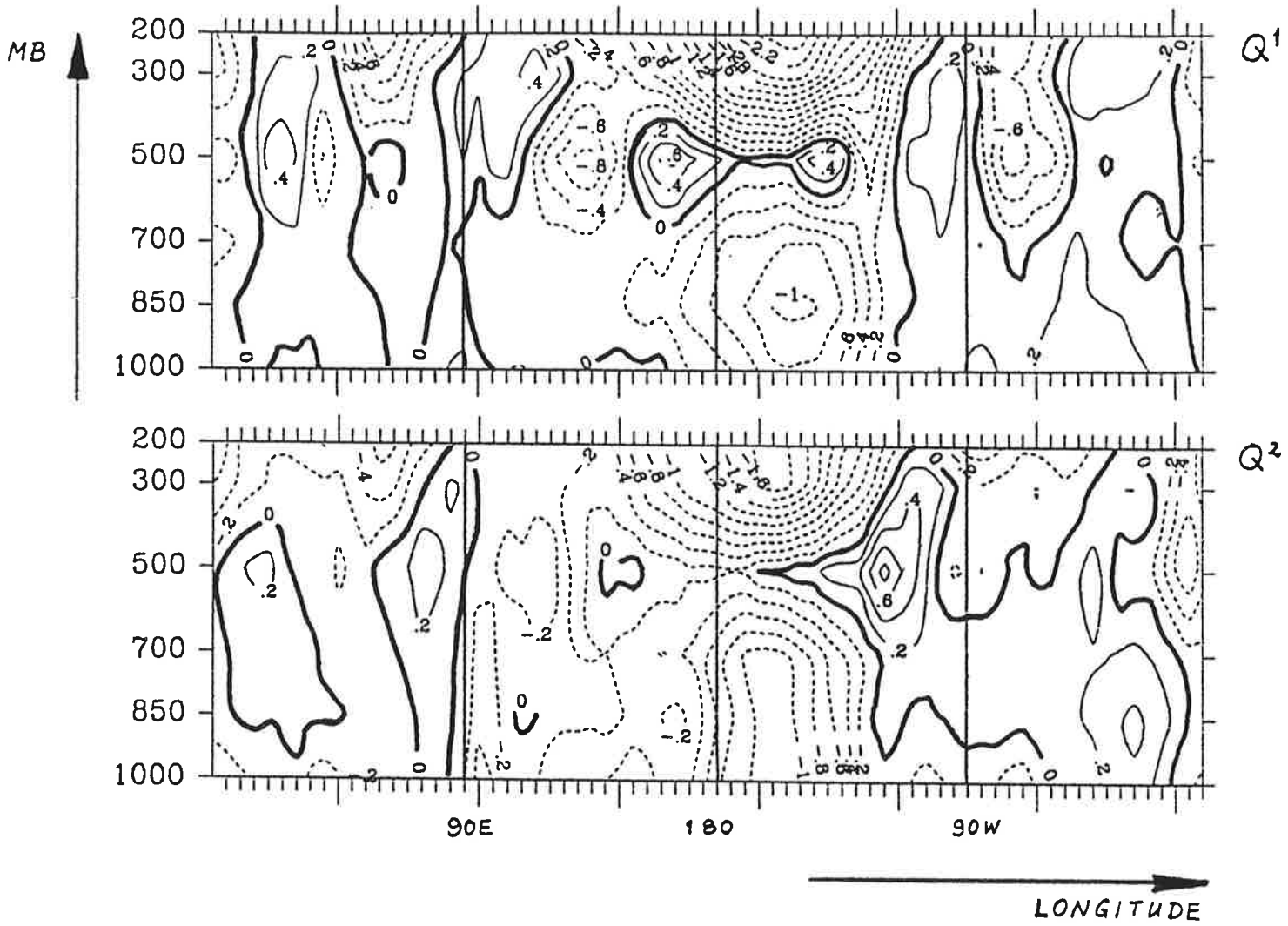

Figure 17:

Longitude-height section of the meridionally averaged (33°N-41°N) associated correlation patterns of the u-winds.

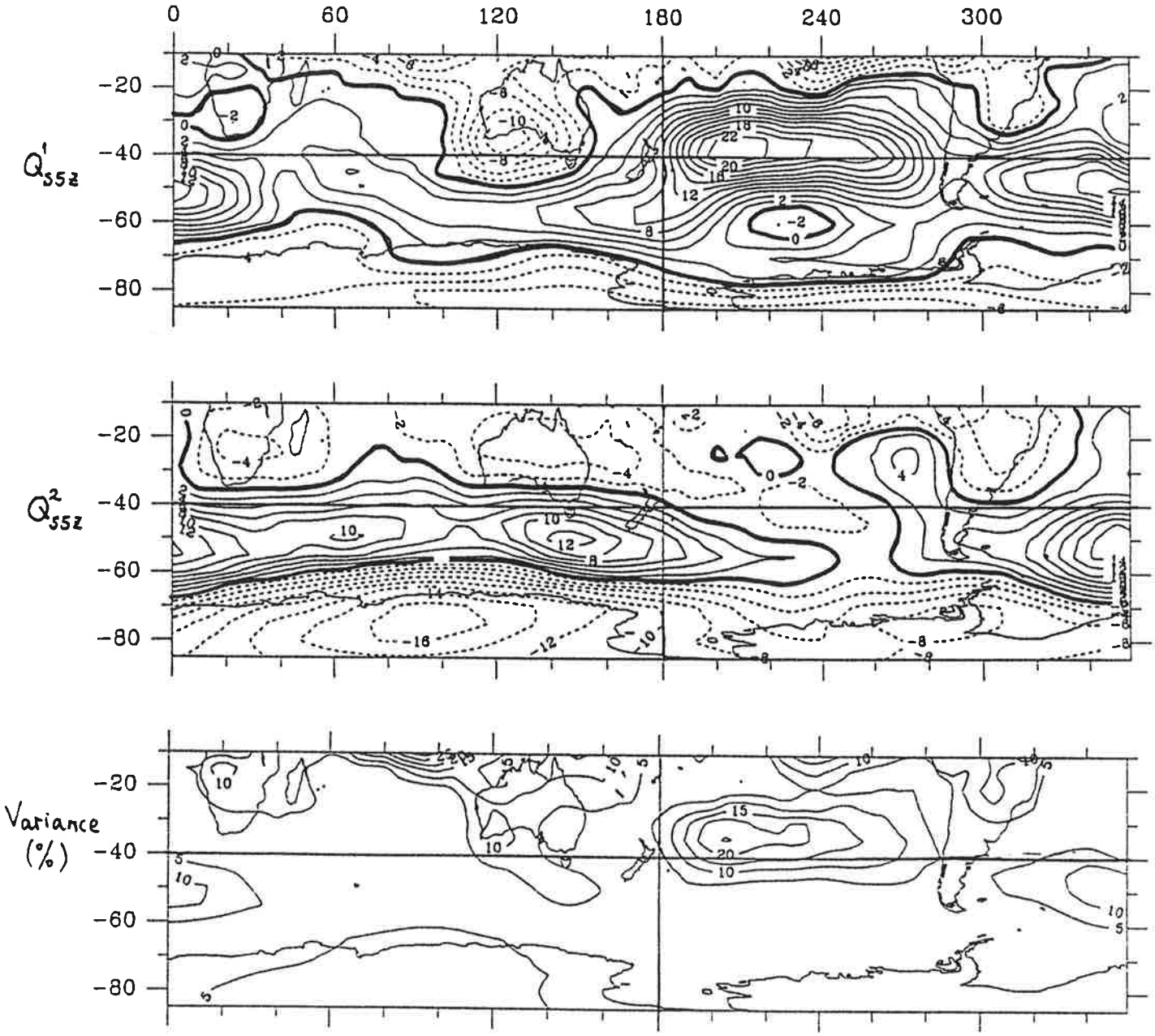

Figure 18:
Associated correlation patterns of Southern Hemisphere 500-mb geopotential height anomalies, Q^1_{SSZ} and Q^2_{SSZ}, and variance explained by these two patterns.

the signal is barotropic. The associated geostrophic winds are westerly (not shown). The explained variance is much smaller in the mid- and high latitudes (maximum values about 5-10%) than in the tropics and subtropics (maximum values about 20-25%).

For the Southern Hemisphere subtropical region, the area with large wind anomalies over the south Pacific at about 30°S (Fig.11 and 12) is investigated in some detail. The associated patterns for the zonal winds are averaged over 24°S-33°S, and plotted in longitude-height section in Fig.19. During the cold phase of the SO easterly anomalies are found in the Southern Hemisphere at about 30°S in the entire troposphere, as in the Northern Hemisphere (Fig.17). By contrast with the Northern Hemisphere, however, the onset phase is characterized by a baroclinic feature over the south Pacific with low level westerly anomalies and high level easterly anomalies.

Air Temperature (AT) and Precipitation (PRC)

The signal in the station air temperature and precipitation data is much less clear than that in the other tropical parameters. The variance explained by the associated correlation patterns from the air temperature data is mostly smaller than 10%, and that from the precipitation data even smaller than 5% (not shown). This effect may be partly due to the fact that station data contain more noise than the analyzed data. In any case the results have to be considered carefully.

A Cold (Warm) Event (Q^1_{AT} and $-Q^1_{AT}$ in Fig.20) is generally connected with anomalous cooling (warming) over most of the continents, except for the eastern part of Australia and for New Zealand. The negative temperature anomalies over the north U.S. could be related to the anomalous anticyclonic flow over the north Pacific (Q^1_{W8}). In the intervening stage (Q^2_{AT}), over most of the land the temperature distribution is quite similar to that in the extreme stage, and only in Australia and New Zealand have the signs of the temperature anomalies changed.

Although the explained variance for the precipitation data is fairly small, the large scale tropical precipitation redistribution during Warm and Cold Events is clearly demonstrated in Q^1_{PRC} and $-Q^1_{PRC}$ (Fig.21). During a Cold

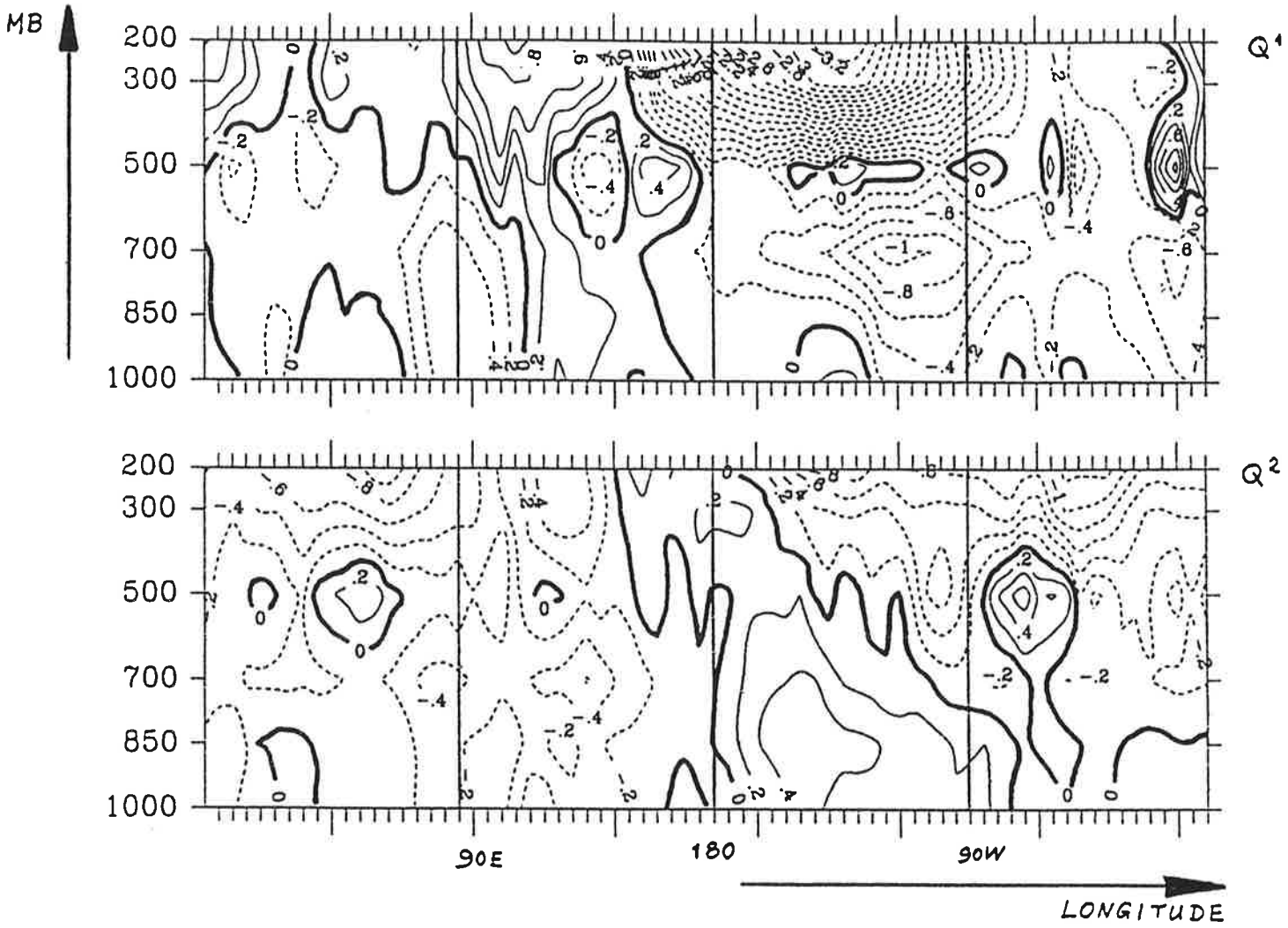

Figure 19:
Longitude-height section of the meridionally averaged (24°S-33°S) associated correlation patterns of the u-winds.

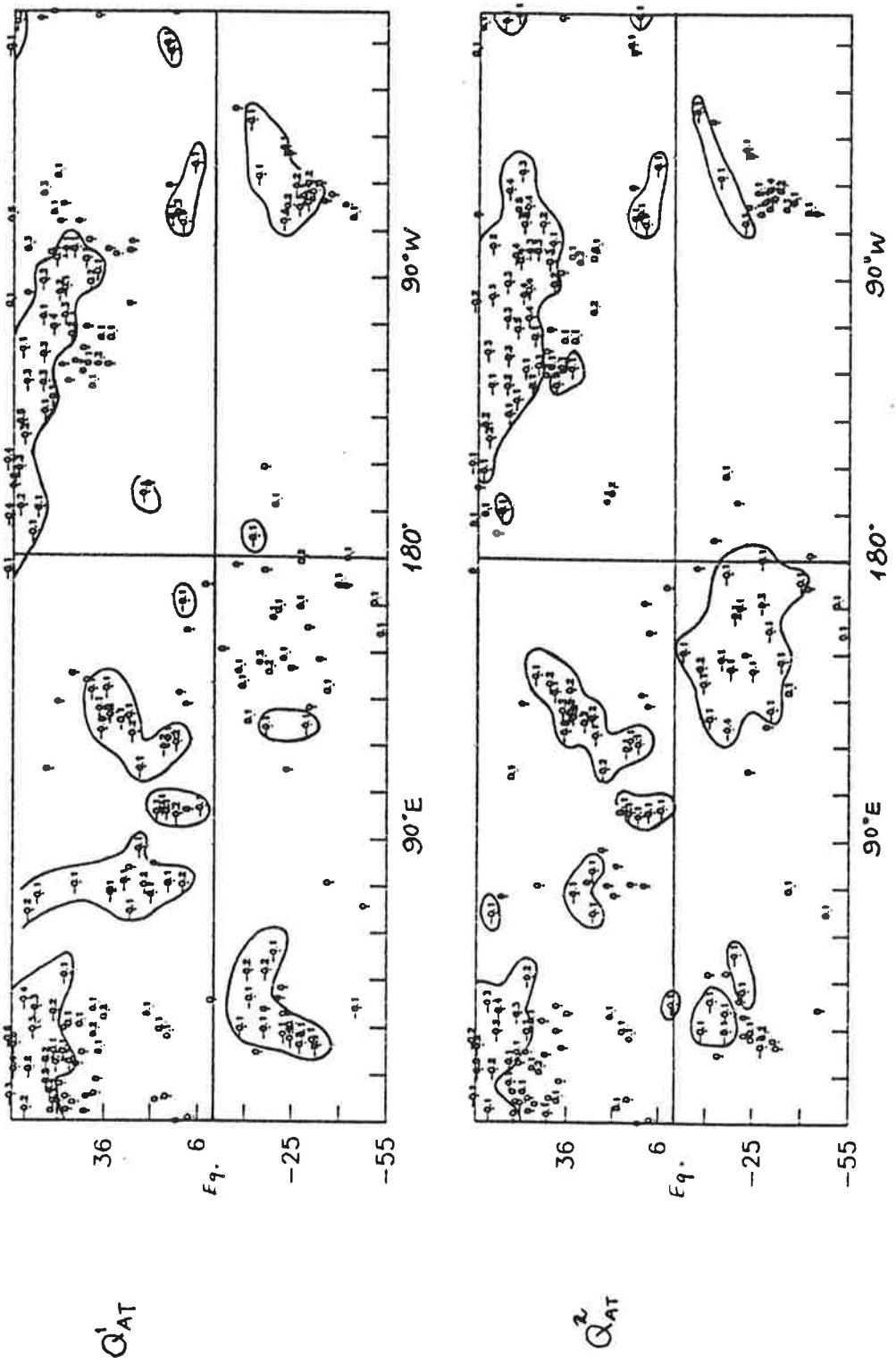

Figure 20:
Associated correlation patterns of station air temperature anomalies, Q^1_{AT} and Q^2_{AT}, and variance explained by these two patterns. °C

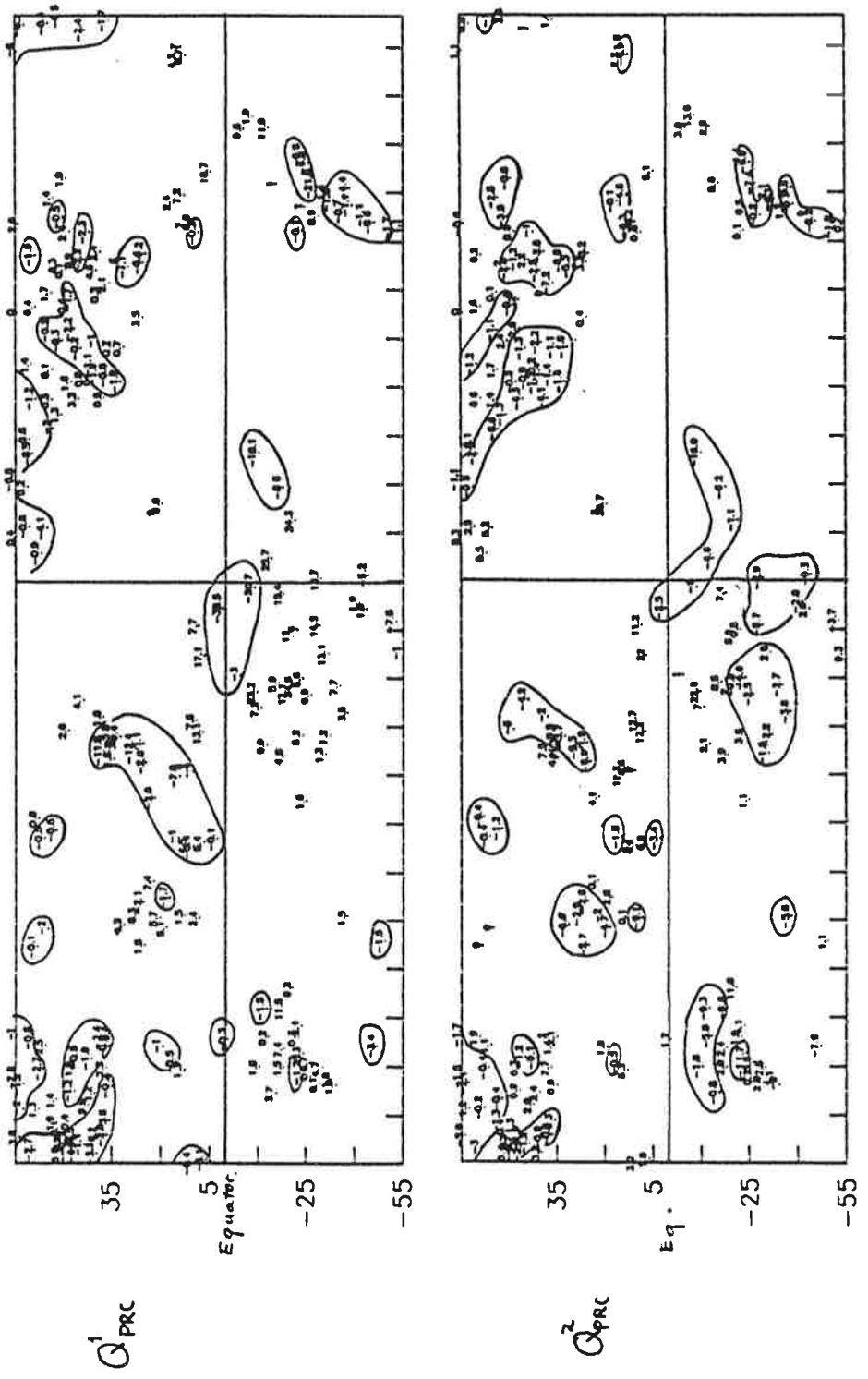

Figure 21:
Associated correlation patterns of station precipitation anomalies, Q^1_{PRC} and Q^2_{PRC}, and variance explained by these two patterns.

Event, positive rainfall anomalies are found over the the west Pacific including the Australian region, and there is less rainfall than usual over the central Pacific. The precipitation anomalies related to the cold (warm) phase of the SO are also found over other land areas, e.g. anomalous wet (dry) conditions over northern South America, the Indian subcontinent and southern Africa, and anomalous dry (wet) conditions over eastern equatorial Africa, southern South America and most of Europe and north America. In the intervening stage (Q^2_{PRC}) following a Cold Event an area of negative rainfall anomalies remains in the central Pacific, but the wet region over the Indonesian region and the west Pacific has moved eastward to about 170°E, indicating a eastward migration of the ascending branch of the Walker Circulation. This result is consistent with other observational studies (e.g. Ropelewski and Halpert, 1987).

Summary: the SO Related Signal in the Other Parameters

The variance explained by the associated correlation patterns is small in the fields of the extratropical wind and height, the air temperature and the precipitation. It reflects the noisy character of the atmosphere and the fact that the SO related signal is weaker in these parameters than in those discussed in the previous sections. Nevertheless the results show some interesting aspects of the SO related variations.

During the extreme phase of the SO, anomalous westerlies/easterlies are found in the entire troposphere near 35°N-40°N and 30°S (Fig.17 and 19). However the anomalous circulations associated with these wind anomalies are different in the Northern and Southern Hemisphere.

In the Northern Hemisphere, a pattern with largest center of action over the north Pacific is found. The results are consistent with numerical studies (e.g. Shukla and Wallace, 1983; Storch and Kruse, 1985) that tropical SST anomalies are capable of producing anomalies at extratropical latitudes. These anomalies exhibit a barotropic vertical structure and are often understood as a Rossby wave propagation with largest anomalies over the north Pacific (e.g. Hoskins and Karoly, 1981). The spatial distribution of these anomalies is named PNA (Pacific/North America) pattern, which is similar to Q^1_{N5Z}.

In contrast to that, the SO-related variability in the Southern Hemisphere mid- and high-latitudes is much more zonally symmetric, and that is consistent with numerical studies (Storch, personal communication) also.

The dominant feature of the SO-related surface temperature is the positive correlation between the SST in the central east Pacific and the air temperature over most of the tropical land mass.

PART: IV THE POP PREDICTION OF THE SOUTHERN OSCILLATION

10. DESIGN OF THE HINDCAST EXPERIMENTS

The oscillation period T in the forecast equation (7) is not derived from the POP's eigenvalue but is taken from the cross - spectral analysis of the two POP coefficient time series $z^1(t)$ and $z^2(t)$ and the SOI time series (Fig.3). Because $z^1(t)$, $z^2(t)$ and the SOI exhibit maximum coherence at 30 months, T=30 is chosen for all hindcast experiments. The time domain filter used to estimate the initial values and the trajectory have approximately the same spectral characteristics as the spectral filter used in Section 3 (see Appendix).

Hindcasts are made for each month from April 1974 to September 1988. The data from 1972 to March 1974 are disregarded because there are too few observations to perform the filtering. Also, the data from the 1950s are not used because of data quality problems. This is illustrated by Fig. 1b, which shows the filtered SOI, Darwin minus Papeete SLP, as derived from station data and from the gridded analyzed data. The deviation of the grid point time series from the station based SOI is substantial in the fifties.

During the hindcast experiment period from 1974 to 1988, the Southern Oscillation is in the warm phase in 1976/77, 1982/83, and 1986/87, in the cold phase in 1975 and 1988 and in the quiet phase in 1978-80 and 1984-86. These ENSO phases could be hindcast up to 2-3 seasons "in advance" throughout the period. The only exception was the cold phase in 1975, which was preceded by irregular conditions, namely the "aborted" El Niño 1974 (see below).

11. CASE STUDIES

In this section we show the hindcasts for four particular phases in some detail. These cases include both the most and least skillful hindcasts (Warm Event 1982/83 and Cold Event 1975/76). Because the 82/83 event is the largest event in the considered period, it might be speculated that the skill of the POP prediction model is mainly due to the correct simulation of the evolution of the 82/83 event. To demonstrate that this is not the case, the hindcasts for the warm phase 1976/77 and for the quiet phase 1985 are shown also. The results are displayed in the two-dimensional z-plane (Figs. 22-24). The two axes in the diagrams refer to the POP coefficients, z^1 and z^2; the solid

(dashed) tilted line indicates the warm phase (cold phase) direction defined by the phase between the POP coefficients and the SOI. The solid curve is the z-trajectory, using the non-symmetric filter (see Appendix), up to the initialization time t_o. The hindcasts, prepared with the observations up to t_o, are indicated by the •-symbol.

The classification into "small", "normal" and "very large" events follows (8). The d(z) = constant contours are given by circles because the covariance matrix *S* is nearly a unit matrix. When the initial value, at t_o, lies outside the 33% circle and the analyzed trajectory propagates clockwise to the solid (dashed) line, a warm (cold) event is predicted to take place; when the trajectory departs from the solid (dashed) line a warm (cold) event is decaying; a trajectory within the "small" area indicates that no events will take place in the near future.

Warm Event 1982/83

Figure 22 shows the predicted evolutions using four initial times, t_o = November 1981, and January, March, and May 1982. The analyzed POP coefficients evolve irregularly with small amplitude until northern spring 1981. In northern summer and fall of 1981 the coefficients are amplified and the trajectory begins to rotate clockwise, which indicates that the process described by the POP is "active". Starting in November 1981 and in January 1982, a weak Cold Event is predicted to peak in January / February 1982, which might be followed by a weak warm event one year later (Figs. 22a and b). Starting in March and May 1982, however, a dramatic intensification is monitored - the initial z-values lie outside the 90% circle - and a very large Warm Event is predicted to peak in January 1983 (Figs. 22c and d).

Cold Event 1975

The prediction of the Cold Event 1975 is less satisfactory. This is demonstrated by Fig. 23 showing the hindcasts initialized in November 1974 and July 1975. Because no data are available before April 1972, non-symmetric

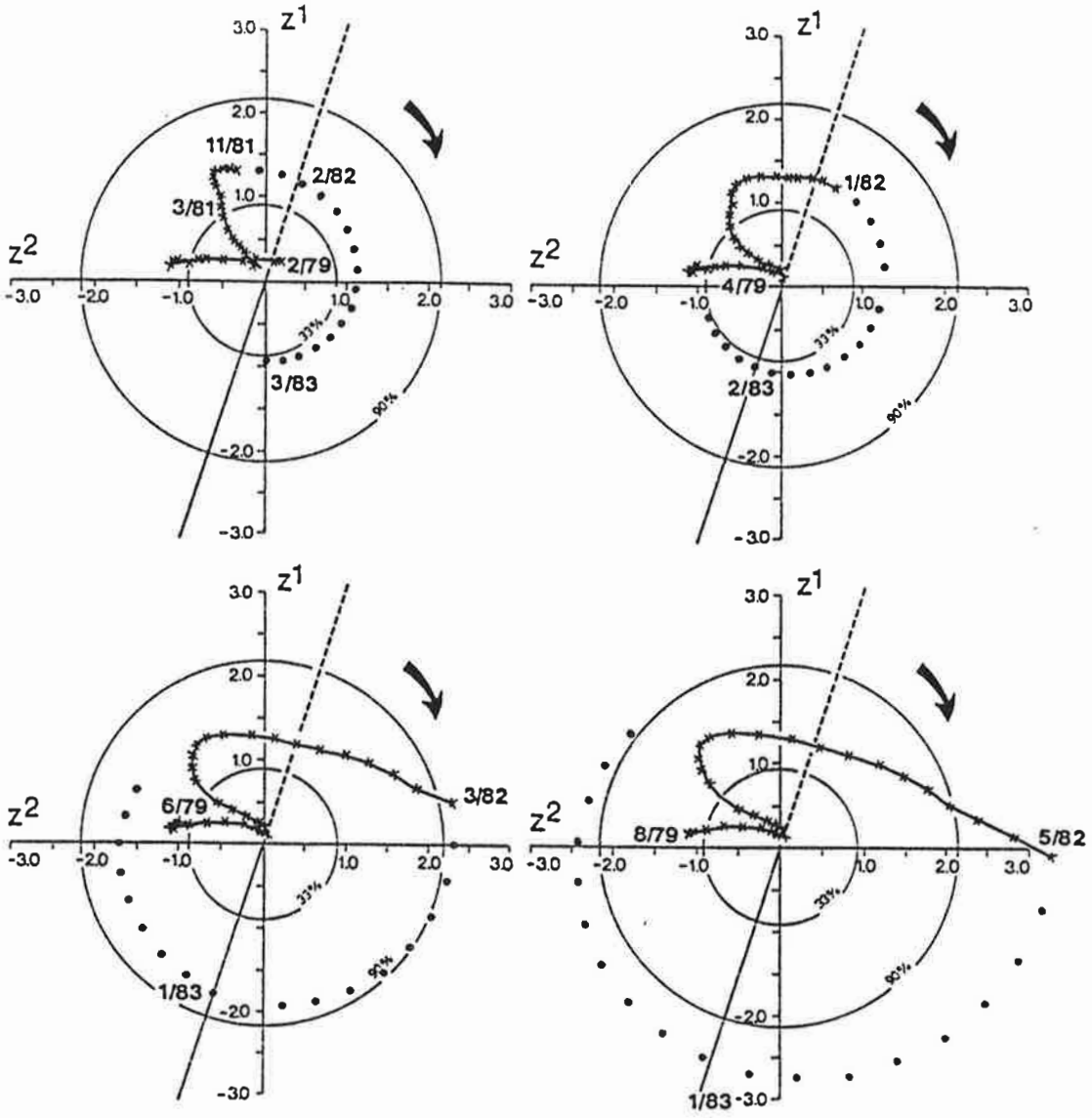

Figure 22:
Results for the hindcast experiments on the 1982 warm event displayed in the two-dimensional z-plane. Initial times t_o = (a) November 1981, and (b) January, (c) March and (d) May 1982.
The two axes in the diagrams refer to the POP coefficients, z^1 and z^2; the solid (dashed) tilted line indicates the "El Niño" ("La Niña") direction defined by the phase between the POP coefficients and the SOI. The solid curve is the analyzed z-trajectory up to the time t_o. The hindcasts, prepared with the observations up to t_o, are indicated by the •-symbol.

If the trajectory propagates clockwise to the solid (dashed) line, a warm (cold) event is predicted to take place. Similarly, moving off the El Niño / La Niña lines is interpreted as the decay of an event. A trajectory which behaves irregularly or which is within the "small" area (given by the inner circle), indicates that no event will take place in near future. A trajectory outside the outer circle indicates the occurrence of a very large event.

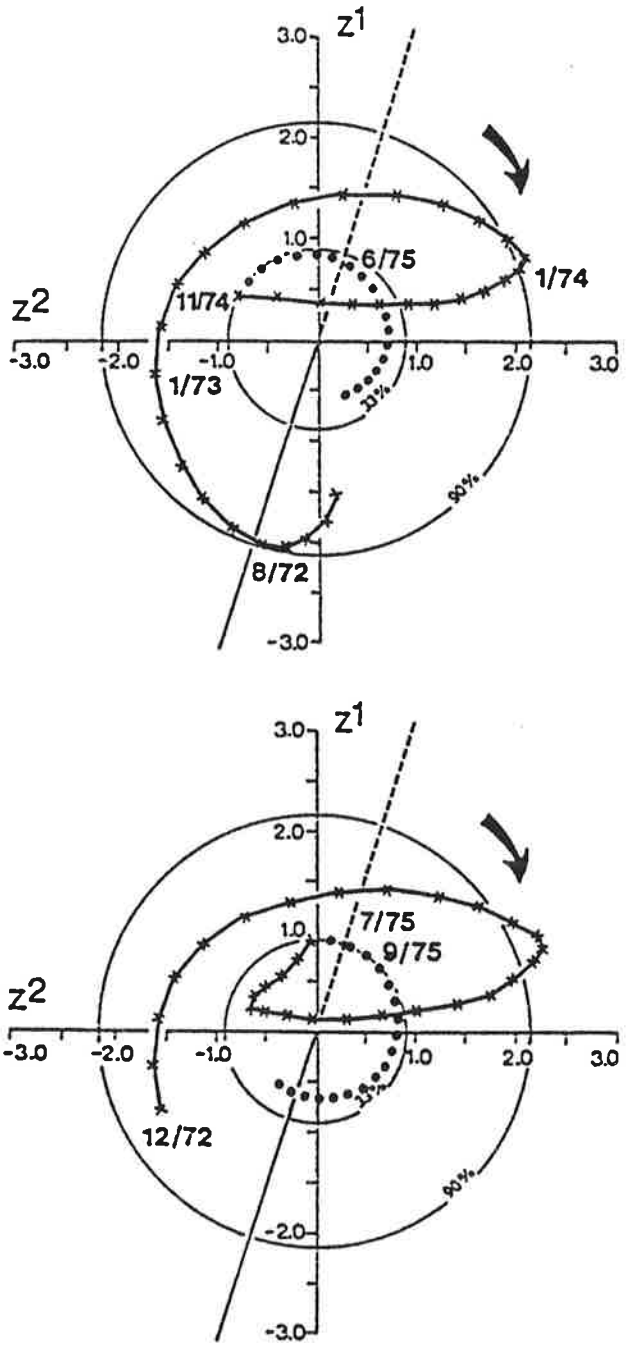

Figure 23:
Results for the hindcast experiments on the 1975 cold event. Initial times t_o = November 1974 and July 1975. In winter 1975/76 the SOI is strongly positive. For description of the diagram, see caption to Figure 4.

filters had to be used to estimate the trajectory at both ends: in 1972 and in 1974.

After having crossed the warm event line in summer 1972 and the cold event line one year later, the trajectory in early 1974 is entering the "quiet phase" stage, i.e. the inner 33% circle, indicating the breakdown of the process. Therefore the November 1974 prediction is that no event will appear in 1975. A correct forecast could only have been made in July 1975, i.e. shortly before the peak phase of the Cold Event, when the process is weakly reflected in the POPs (Fig. 23b).

Warm phase 1976/77

As already mentioned in Part II, the warm phase 1976/77 lasted over one year and is characterized by two maxima of the unfiltered SOI at the ends of 1976 and 1977. Using data until May and August 1976, the POP model predicts a Warm Event at the end of 1976 and in the beginning of 1977 (Fig.24). When data until October 1976 is used, the POP model correctly indicates that the Warm Event 1976/77 will not diminish as usually happens, but will amplify again at the end of 1976.

Quiet Phase 1985

The hindcasts using data up to September 1984 and January 1985 are shown in Fig. 25. In these hindcasts the analyzed POP trajectory enters and stays within the 33% circle at the end of 1983. The system is correctly diagnosed as being in a quiet phase, and the prediction was that no event, cold or warm, was to be expected within the near future.

12. HINDCAST SKILL OF THE POP MODEL

To assess the overall capability of the POP prediction scheme, a hindcast skill S^P is derived via (9) from all hindcast experiments. The low pass filtered SOI (Fig. 2b) is used as the observed statistic O(t). For the predictions, the statistic P(t) is the predicted SOI.

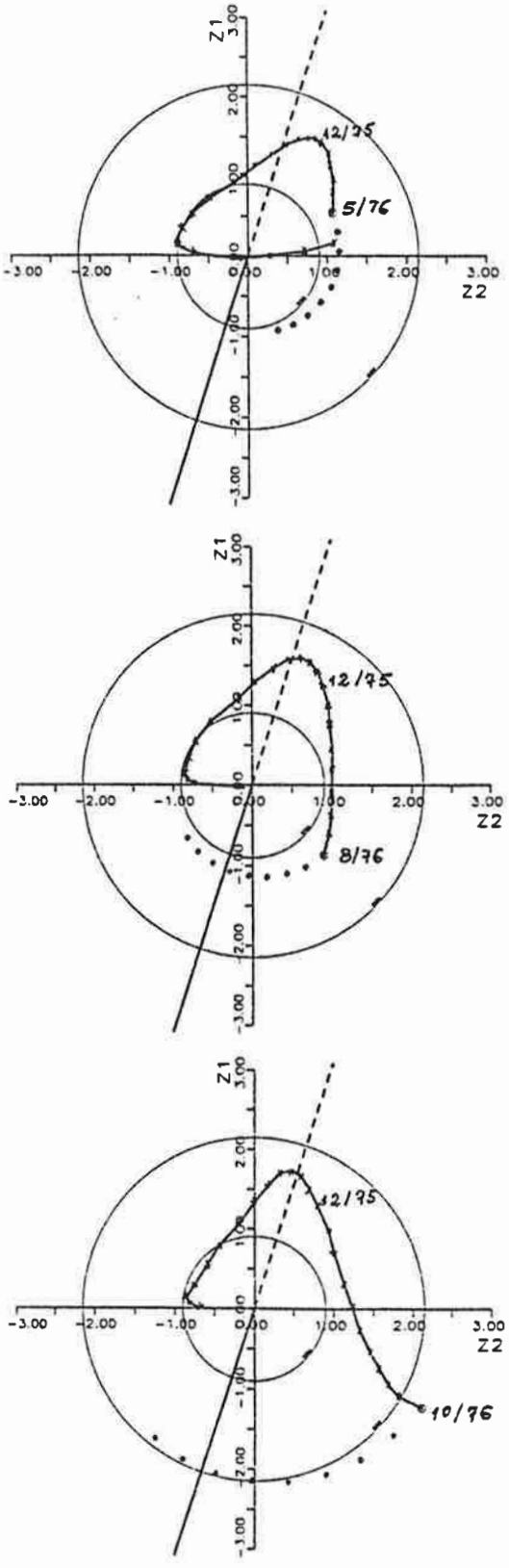

Figure 24:
Results for the hindcast experiments on the 1976/77 warm event. Initial times t_o = May, August and October 1976. At the ends of 1976 and 1977 the SOI is strongly positive. For description of the diagram, see caption to Figure 4.

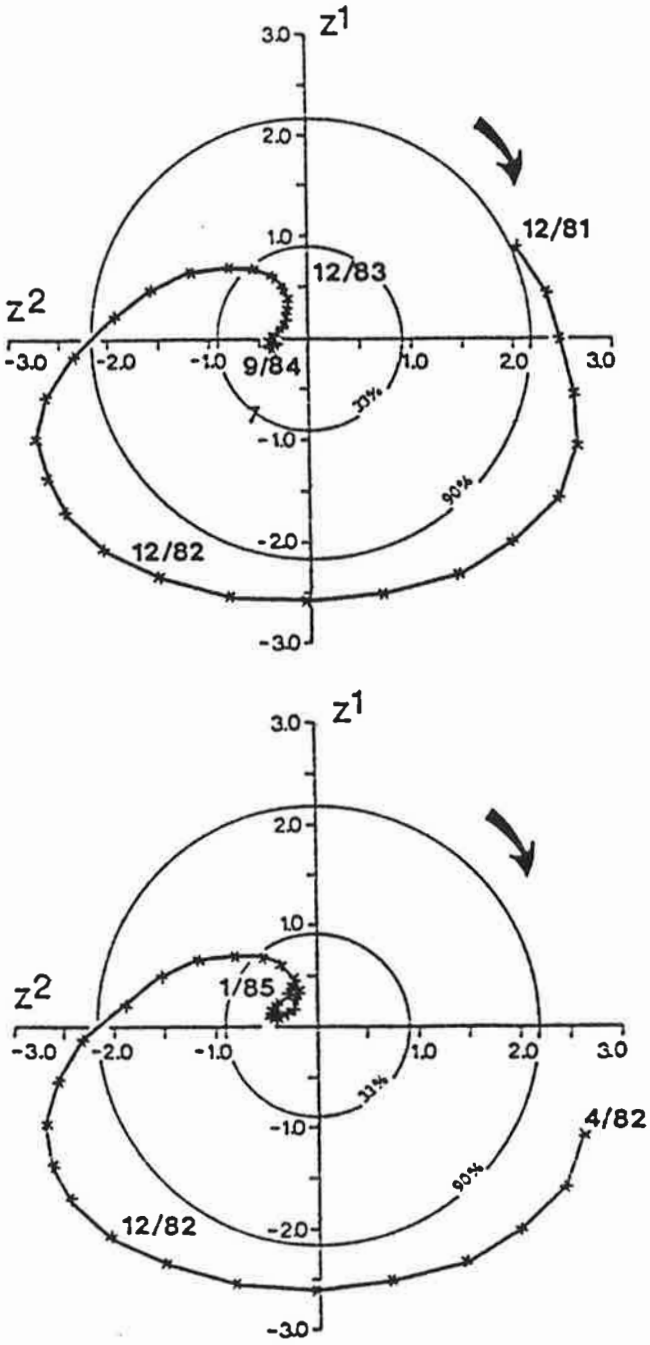

Figure 25:

Results for the hindcast experiments on the 1985 quiet phase. Initial times t_o = September 1984 and January 1985. During 1984 and 1985, the SOI was small. For the description of the diagram, see caption to Figure 4.

The persistence forecast is used as a reference in order to assess the skill of the POP hindcasts. The unfiltered SOI is known to be affected by month-to-month variations which are not related to the state of the Southern Oscillation but reflect high frequency variabilities, e.g., the activity of the tropical 30-60 day wave. Therefore, the control forecast is based on 3-month running means, i.e.:

$$(10) \qquad P_{pers}(t_o+\tau) = P_{pers}(t_o) = \frac{SOI(t_o)+SOI(t_o-1)+SOI(t_o-2)}{3}$$

As a second reference forecast scheme we use the conventional ARMA (1,7;1) model derived from the monthly SOI by Chu and Katz (1985):

$$(11) \qquad P_{ARMA}(t+1) = 1.011 \cdot P(t) - 0.115 \cdot P(t-6) + \alpha_{t+1} - \theta_1 \alpha_t$$

The white noise forcing terms, α_{t+1} and $-\theta_1 \alpha_t$, are disregarded when performing the predictions.

The hindcast skill S^P at each time lag τ=0-19 months, as calculated for the POP scheme, for persistence according to (10), and for the ARMA model according to (11), is shown in Fig. 26. Persistence is clearly better for the "now cast" and forecasts for lags $\tau \leq 2$ months. After that, the POP scheme is superior; after 9 months, no correlation exists between persistence and observation, while the correlation between $P_{pop}(t)$ and $O(t)$ is still about 40%. The ARMA model is somewhat better than the the persistence but is clearly worse than the POP model.

The fact that persistence is better than the POP scheme in the first months is expected. One reason is the non-symmetric filtering to obtain initial values for the POP prediction. The second reason is the low-frequency variability of the SO which is persistent on a time scale of a few months. The time scale of changes of the state of the SO is larger than one season ($T/4 \approx 8$ months), and it is here that the POPs are most successful in describing these changes.

The difference between the POP scheme and the conventional ARMA model is that the POP scheme makes use of the full fields by projecting these onto a smaller set of dominant patterns. The POPs describe a propagating feature in the SLP field whereas the ARMA describes the evolution of one univariate time series.

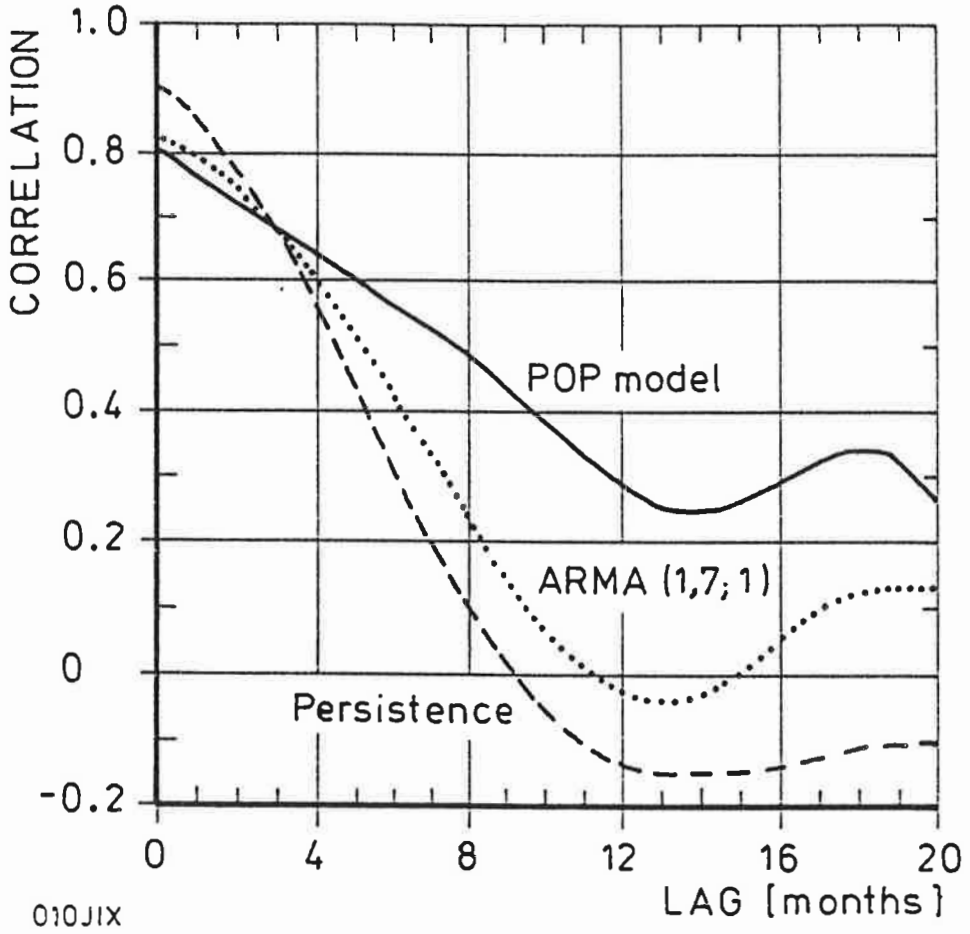

Figure 26:

Correlation skill S^P, according to (9), of the prediction of the Southern Oscillation Index. Solid curve: POP prediction. Dashed curve: 3-month mean persistence. Dotted curve: ARMA(1;7,1) from Chu and Katz (1985)

The intermediate state, P^2, which plays an important role in the development of an ENSO event, cannot be described by the univariate SO index.

It has to be kept in mind that the presented skill scores are hindcast scores. If the time series were sufficiently long one might derive the artificial skill by cross validation. For that purpose one would have to delete, for example, 2 year episodes from the entire data set, to design a POP model with the remaining data and to calculate the skill for the 2-year episode that would represent independent data. In the present case, however, this is not possible because of the shortness of the time series and the necessity of low frequency filtering. If a 2-year interval were disregarded, a discontinuity at the ends of the interval would be introduced. This discontinuity would distort the time evolution up to one year before and after the 2-year interval (as mentioned in the Appendix) so that about 4 years of information would be lost for the POP analysis. In view of the limited reliability of the 1951-58 data, a loss of 4 years of data, particularly if the lost period includes events, is not acceptable for the POP analysis.

I believe, however, that the artificial skill is not substantial. As mentioned before, the POP forecast scheme is not based on a least square fit. Experiences in another study (Storch and Xu, 1989), with sufficiently long time series, support this view. A small amount of artificial skill might be introduced by inferring the oscillation period from the cross - spectral analysis of the POP coefficients and the SOI.

PART:V DISCUSSIONS AND CONCLUSIONS

13. THE SOUTHERN OSCILLATION CYCLE

In the previous sections pairs of patterns P^1/P^2, Q_v^1/Q_v^2 have been identified which represent the SO-related signal in the key variable and in other oceanic and atmospheric variables **v**. The notion that the Southern Oscillation can be described as a damped oscillation in the 2-dimensional space spanned by $\begin{pmatrix} P^1 \\ Q_v^1 \end{pmatrix}$ and $\begin{pmatrix} P^2 \\ Q_v^2 \end{pmatrix}$ is supported by the following arguments.

First, the SO characteristic patterns in SLP, SST, sea level and winds described by $\begin{pmatrix} P^1 \\ Q_v^1 \end{pmatrix}$ are consistent with other investigations. The coefficient $z^1(t)$ is significantly in phase and $z^2(t)$ 90° out-of-phase with the traditional SOI (Fig. 3). It indicates that $\begin{pmatrix} P^1 \\ Q_v^1 \end{pmatrix}$ represents the extreme phase and $\begin{pmatrix} P^2 \\ Q_v^2 \end{pmatrix}$ the onset phase of the SO.

Secondly, additional data are used to make sure that the onset phase of the SO is not the artifact of the POP analysis technique. They are the SLP time series in the anomaly centers in P^1 represented by Darwin and Papeete in P^1, and the anomaly center in P^2 represented by Raoul island (position marked in Fig.4). The pressure difference between Darwin and Papeete, i.e. the traditional SOI, and the pressure over Raoul Island are cross - spectrally analyzed. The results are shown in Fig.27 for the period from 1951 to 1982. There is a spectral peak at 30-40 months in the coherence spectrum indicating the oscillatory acpect of the SO. The precursor role of the SPCZ anomalies is also supported by a methodologically different investigation using many long time series (Zwiers and Storch, 1989).

Finally, the hindcast skill, which is much higher than the skill of a traditional ARMA model, substantiates also the large scale cyclic characteristic of the Southern Oscillation phenomenon.

Thus, the POP analysis leads to a concept of the Southern Oscillation which is fundamentally different from the traditional notion that the SO is a standing oscillation readily monitored by an index such as Darwin minus Papeete SLP.

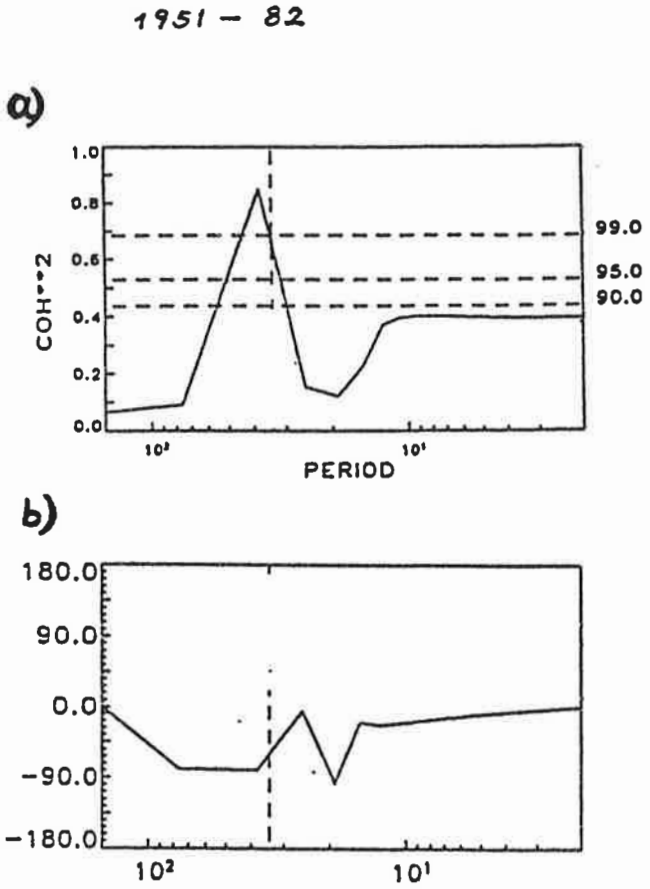

Figure 27:

a) Coherence spectrum between SOI and pressure anomaly over Raoul Island.
b) Phase spectrum between SOI and pressure anomaly over Raoul Island.

Instead, the POP model identifies the SO as a large - scale eastward propagating feature in the atmosphere and ocean (as reflected in many parameters e.g. SLP, winds, sea level and upper layer temperature), which is insufficiently monitored by the SOI alone. This result, especially the atmospheric aspect of this propagating feature, is in accord with some other studies, e.g., Barnett (1985,1988), van Loon and Shea (1985, 1987), Gutzler and Harrison (1987), and Storch et al. (1989a,b).

14. THE EQUATORIAL ATMOSPHERE-OCEAN INTERACTION

As already shown, the SO related variabilities in the tropical atmosphere-ocean system can be described as a damped oscillation in the two-dimensional space spanned by pairs of patterns, especially by Q_0^1/Q_0^2 in Fig.9 and Q_U^1/Q_U^2 in Fig.15. The amplitude of anomalies during such a cycle is not uniform, but has larger values in the extreme warm and cold phases than in the transition phase. It seems that different processes are going on at different stages of the oscillation. In the coupled atmosphere/ocean system, the surface winds determine principally the oceanic circulation and therefore the equatorial SST pattern, and the SST pattern on the other hand directly influences the atmospheric circulation. Such air-sea interaction might cause variations in the coupled system. In the following the air-sea interaction at different stages of the Southern Oscillation cycle is considered in some detail.

a) The atmosphere-ocean interaction during the extreme phase of the SO

During a Cold Event, positive SST anomalies are located in the west Pacific (Q_{SST}^1). Corresponding to that, low level convergent and upper level divergent motions are found in the tropical atmosphere over this area (Q_U^1), and these are connected with stronger than normal low level easterlies east of the anomalously warm water. The tropical Pacific reacts to these wind anomalies, and generates stronger than normal SEC (Q_0^1), which advects more warm surface water into the west Pacific. Positive feedback is therefore taking place in the interaction between the ocean and the atmosphere in this region. Consequently the initial anomalies, i.e. the low-level convergent and upper level divergent motions and also the positive SST anomalies and the anomalous

westward surface current, are intensified.

A similar interaction process occurs during a Warm Event, when anomalous warm water is located in the central and east Pacific. In this case the anomalous westerlies west of the warm water are responsible for the interaction process in the atmosphere and ocean. The westerly wind anomalies cause not only an anomalous eastward surface current, which advect west Pacific warm water into the central and east Pacific, but also anomalous downwelling, which prevents the upward drawing of colder subsurface water. At the end, the east Pacific becomes warmer, and the initial atmospheric anomalies become stronger.

b) The atmosphere-ocean interaction during the intervening stage of the SO

As described in section 8.1, the eastward movement of the subsurface ocean temperature anomalies is caused by the reduction of the upwelling in the central Pacific and the advection by anomalous eastward surface current in the west Pacific (Q_0^2 in Fig.9). From Q_U^2 (Fig.15), it is clear that this anomalous oceanic circulation is produced by the anomalous atmospheric circulation involving low level westerlies over the west Pacific. But, as indicated by Q_{SST}^2 and Q_{ST}^2, the ocean at this stage does not produce any notable sea surface temperature anomalies, therefore the atmosphere is not responding to the ocean at this stage.

It is concluded that during the Southern Oscillation cycle the air-sea interaction plays an important role. During the extreme phases the interaction does have the effect of strengthening the initial anomalies, i.e. positive feedback is taking place between the atmosphere and the ocean; whereas in the intervening phase the ocean is responding to the changes in the atmospheric circulation, but the atmosphere is not responding to the changes in the ocean. Therefore no positive feedback is taking place at the intervening stage. The pattern of air-sea interaction that exhibits positive feedback, was first suggested by Bjerknes (1966), and also proved by many numerical studies. The other pattern, identified explicitly by the POP model as a dominant feature of the intervening stage of the SO, is the important finding of this paper.

15. THE OTHER POSSIBLE MECHANISMS

In the previous section the tropical air-sea interactions during the eastward migration were considered. The question to be asked now is whether processes that are not directly involved in the equatorial air-sea interaction could also influence this cyclic evolution of the coupled system. There are two candidates: one is processes outside the tropical atmosphere, which could modify the Walker Circulation; the other is oceanic wave dynamics, which could interact with the tropical oceanic circulation.

a) The possible mechanisms for modifying the Walker Circulation

During a Cold or Warm Event, besides the strong SST signal in the central and east Pacific, SST signal with opposite sign are found in the north and south Pacific and the western most part of the ocean (Fig.5). Luksch et al. (1989) demonstrated that this anomalous SST distribution in the north Pacific is forced by the anomalous wind stress and heat flux associated with the atmospheric circulation over that region (Q^1_{SLP}). It is therefore reasonable to assume that south Pacific SST anomalies are also forced by the anomalous atmospheric circulation in the south Pacific as shown in Q^1_{SLP}.

It is suggested that the off-equatorial SST anomalies could in turn interact with the atmosphere and consequently modify the atmospheric circulation. Van Loon and Shea have shown that the SST anomalies in the south Pacific are more efficient at influencing the atmosphere than the SST anomalies in the north Pacific. In the mean state the west Pacific is characterized by the warm SST and two convective regions: the ITCZ and SPCZ. It has been shown (van Loon and Kiladis, 1988) that the ITCZ is mainly in the region between 5°N and 10°N mostly west of the dateline, while the SPCZ expands from a zonally-orientated band of rainfall at about 10°S in the southern winter to a wide region of heavy precipitation with its axis orientated northwest-southeast from New Guinea into the south Pacific in the southern summer. Considering again that the region of positive SST anomalies in the south Pacific is much larger than that in the north Pacific in Q^1_{SST}, it is reasonable to assume that the air/sea interaction is much stronger in the south Pacific than in the north Pacific.

Van Loon and Shea speculated further that the positive SST anomalies in the

south Pacific in Fig.5, which are probably associated with the anomalous atmospheric circulation, could result stronger than normal convection. As substantiated by a numerical experiment (Storch et al., 1988), this anomalous convection is associated with negative SLP anomalies in the southwest Pacific and anomalous westerlies over the tropical west Pacific. The results of the POP analysis (Q^2_{SLP} and Q^2_U) are consistent with these studies. Furthermore the baroclinic feature over the south Pacific (Fig.19), indicating intensified convective activities with cyclonic flow at low level (Q^2_{W8}) and anticyclonic flow at high level (Q^2_{W2}), also supports the hypothesis of van Loon and Shea.

At the end of this air-sea interaction over the SPCZ, the low level convergence region of the Walker Circulation over the Indonesian region could be modified and begin to move into the west Pacific.

Another hypothesis, operating with anomalous Eurasian snowfall and its role in modify the Eurasian summer monsoon and also the Walker Circulation, was proposed by Barnett (Barnett, 1985; Barnett et al., 1989). To check this hypothesis, the associated correlation patterns are calculated for the Northern Hemisphere snow data (not shown). The results indicate only the anomalous snow-cover frequency, but not the anomalous snow amount. The explained variance is about 1-2% in most regions. Above normal snow-cover frequency is found in Q^1_{SNOW} and Q^2_{SNOW} over the west part of Eurasia and North America, where the explained variance is about 5%. Large negative air temperature anomalies are found over Eurasia and North America at that time also (Fig.20). These anomalous conditions could force anomalous Indian and southeast Asian monsoon circulation and further modify the Walker Circulation. But the associated anomalies are very small.

b) Oceanic wave activities

The only suitable data for investigating the oceanic wave dynamics are the sea level data. In Fig.28 the evolution of sea level anomalies along the equator and along 10°N and 20°N are demonstrated. It shows a strong eastward propagating signal along the equator, a nearly standing feature along 10°N, and a weak westward propagating signal along 20°N. It is interesting to see that the positive (negative) sea level anomalies along the equator begin to move eastwards from the western boundary after the 20°N positive (negative)

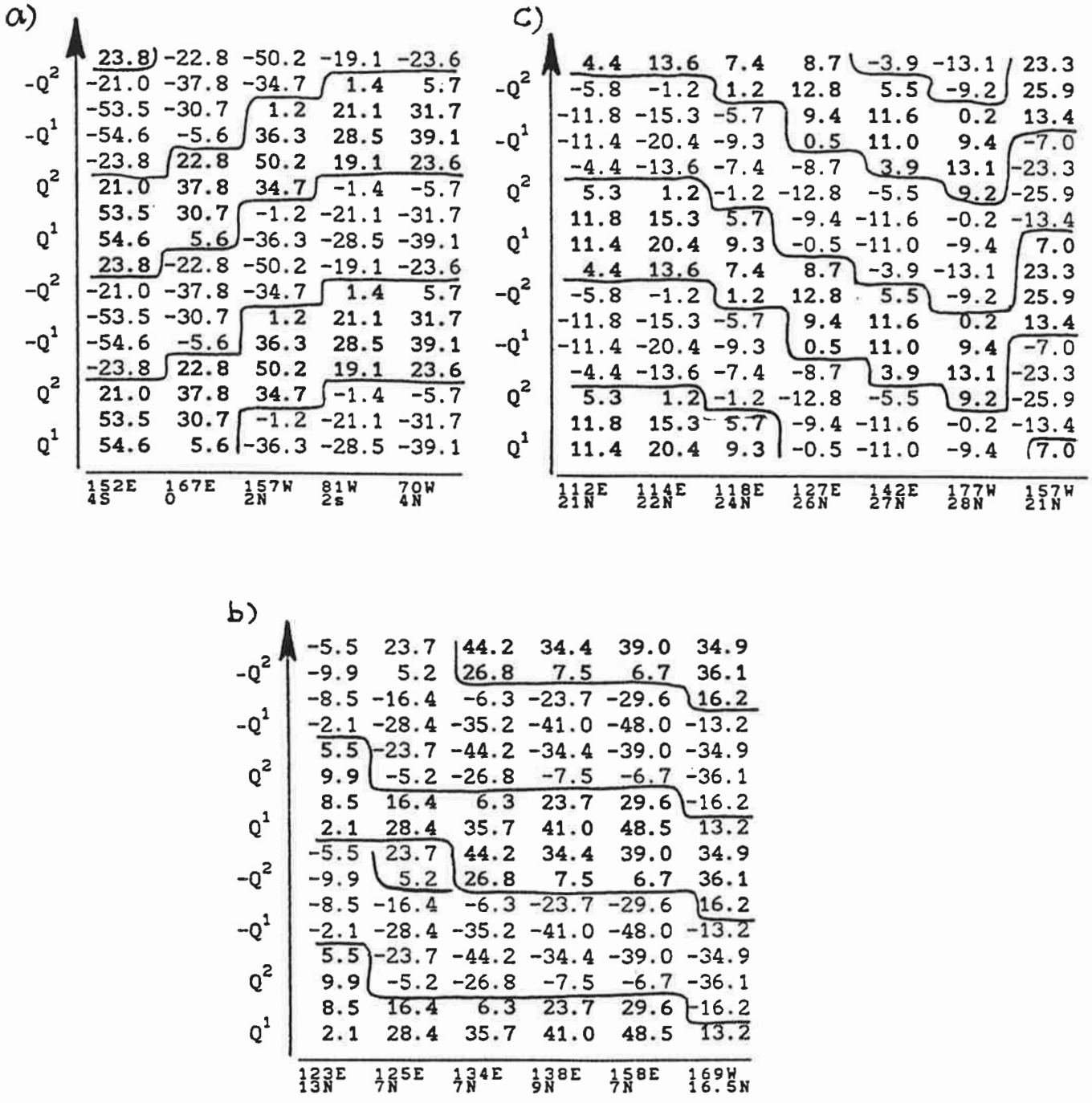

Figure 28:
Hovmoeller diagram of Sea level anomalies along a) the equator, b) 10°N and c) 20°N.

sea level anomalies have already reached the western boundary. More data are required to study the effect of the off - equatorial wave activities.

It is concluded that the results of the POP analysis do not contradict the already existing hypotheses. However, the question of which hypothesis can describe the most important process cannot be clarified by the POP analysis technique.

16. ANNUAL CYCLE AND ENSO CYCLE

Many observational studies (e.g. Rasmusson and Carpenter, 1982) suggest that ENSO is strongly locked to the annual cycle. Our analysis technique did not address the question of whether the POP model is phase-locked to the annual cycle. To answer this question I sorted the complex POP coefficient time series (Fig. 1a) z(t) into eight classes: the complex plane is subdivided into eight regions, K_1, K_2, ...K_8. Each region is a 45° angular segment, so that all segments are of equal area. K_1 contains all active states with phase angles δ of $\frac{9}{8}\pi < \delta < \frac{7}{8}\pi$, K_2 is given by $\frac{7}{8}\pi < \delta < \frac{5}{8}\pi$, and so forth. So, K_1 covers all states described by $-\mathbf{p}^2$, K_2 intermittent states between $-\mathbf{p}^2$ and $\mathbf{p}^1$, K_3 $\mathbf{p}^1$, etc.

A frequency table of z(t) according to class and calendar month is given in Fig. 28. The number of samples available to estimate the frequencies is fairly small so that the results should be treated with caution. In spite of these limitations, however, Fig. 9 clearly demonstrates that the ENSO cycle, as described by the POP model, is locked to the annual cycle (as indicated by the tilted line). The intermittent stages prior to an SO event, e.g. K_1/K_2 and K_4/K_5, tend to emerge in southern fall. The peak phases, $K_3 = \mathbf{p}_1$ and $K_7 = -\mathbf{p}_1$, are most frequent in southern winter and spring. Thus our analysis confirms the well known result that the Southern Oscillation is linked to the annual cycle.

17. PREDICTIONS

The concept of a natural oscillator, described in the reduced system spanned by $Q^1_{A/O}$ and $Q^2_{A/O}$, offers a conceptually simple way of predicting the state of

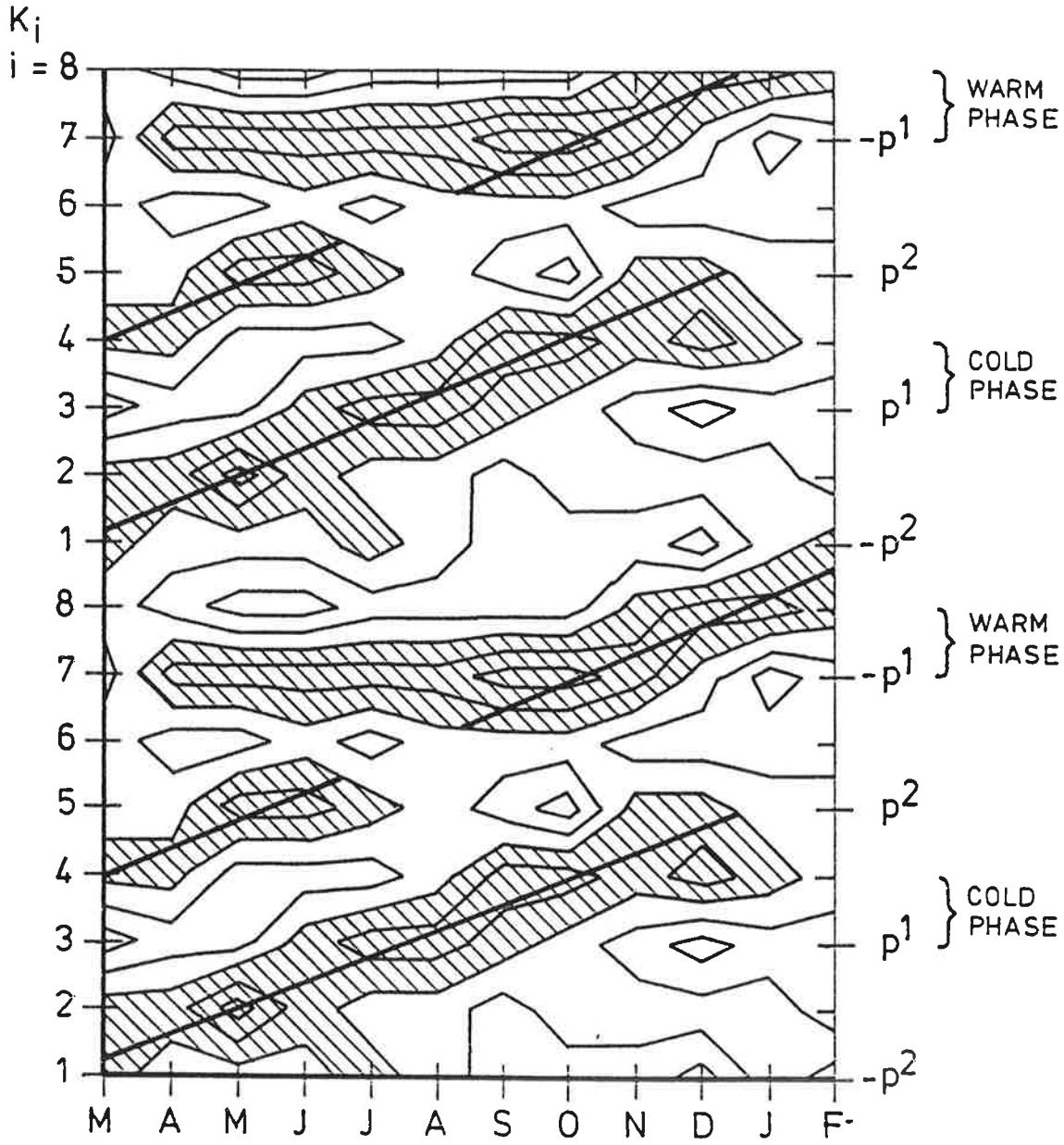

Figure 29:

Frequencies of the complex POP coefficients in class K_i (vertical axis) appearing in a calendar month (horizontal axis). To obtain a clearer picture the frequencies for two consecutive POP cycles are shown.
For the detailed definition of the classes see text. Each of the 8 classes covers a 45° segment; the connection between classes and the appearance of the patterns $\mathbf{p}_1$, $-\mathbf{p}_1$, $\mathbf{p}_2$ and $-\mathbf{p}_2$ is indicated by the labels on the right.
Contour interval is 1. Inside the hatched area, the frequencies are 3 and more.

the SO. The relevant point exploited in the prediction technique is the fact that the trajectory, defined by the POP coefficients in the two-dimensional space, has some "inertia" and that future points of the trajectory may be guessed by simply prolonging the trajectory. Thus the POP prediction is based on a "persistence of motion", in contrast to the "persistence of state" in a conventional persistence model. Therefore the POP prediction scheme is likely to be more successful in indicating the general evolution of the SO than in describing the details, e.g., anomalous SST averaged over certain areas. Also, the POP model is not able to predict a change from the "quiet phase to the "active phase".

It was shown by the overall skill and the case studies that the POP prediction scheme is able to predict the state of the SO for 2 to 3 seasons in advance. One has to keep in mind, however, that all forecasts considered were made in the hindcast mode. Therefore it might be possible that the level of skill is in part contaminated by an artificial skill, even if the forecast scheme is not based on a least square fit.

For a lead time of more than one season the POP "persistence of motion" has a higher *hindcast* skill than the traditional "persistence of state" forecast. The scheme fails only in one case, the Cold Event of 1975. In 1974/75, the ENSO process broke down (the "aborted" 1974/75 El Niño) but became reactivated in a relatively short time. Such a behavior clearly cannot be described by the linear POP model, as was mentioned above.

SO predictions based on statistical models have been made by Barnett (1984) and Graham et al. (1987b). Their approaches differ from ours with respect to both the predictors considered and the domain: tropical wind field (area averaged, Barnett, 1984; or gridded, Graham et al., 1987) and global SLP (Graham et al., 1987). These approaches are also based on different hypotheses. The tropical wind models consider the evolution of the tropical wind system and equatorial waves generated by remote wind forcing; the global SLP model focuses on the eastward movement of Indo-Pacific SLP anomalies. In contrast, our model uses nontropical predictors - Southern Hemisphere SLP - and makes use of the SPCZ hypothesis suggested by van Loon and Shea (1985 and 1987). Interestingly, our predictions seem to have a skill that is comparable to that of the other stochastic schemes, in spite of the exclusion of the

tropical area. This might be an indication that the oscillatory "Southern Oscillation" climate mode is not confined to the tropical region.

Acknowledgements

I wish to express my gratitude to Hans v. Storch and Harry van Loon for their inspiration and encouragement. I am also indebted to Mojib Latif for helpful discussions and for supplying me with the OGCM data. The work was in part financed by the European Community Climate Program under grant EV4C - 0035 -D(B).

Appendix

Time filters in frequency domain and in time domain

A time series $\mathbf{x}(t)$ may be filtered in time domain and in frequency domain. In the following I briefly summarize the two well known concepts.

In the time domain the filter may be expressed as a linear operator

$$\tilde{\mathbf{x}}(t) = \sum_{j=-m}^{m} a_j x(t+j\Delta t) \tag{A.1}$$

If $\mathbf{x}(t)$ is a periodic function with the Fourier expansion

$$\mathbf{x}(t) = \sum_{\omega} \alpha(\omega) exp(i\omega t)$$

the filtered time series is

$$\tilde{\mathbf{x}}(t) = \sum_{\omega} \alpha(\omega) \cdot H(\omega)\ exp(i\omega t)$$

with

$$H(\omega) = \sum_{j} a_j exp(ij\omega\Delta t) \tag{A.2}$$

This way of calculating $\tilde{\mathbf{x}}$ is called *time domain filtering*. If the time domain filter is symmetric, i.e. $a_j = a_{-j}$, only the amplitudes of the Fourier components are modified but the phases are unchanged.

The same result, $\tilde{\mathbf{x}}$, may obtained by deriving from the raw time series $\mathbf{x}$ the Fourier coefficients $\alpha(\omega)$, by multiplying the Fourier coefficients by the numbers $H(\omega)$, and by reconstructing the time series with the modified Fourier coefficients, $\alpha(\omega) \cdot H(\omega)$. This approach is called *frequency domain filtering*.

For each time domain filter there is an equivalent frequency domain filter, and frequency domain filters may be approximated by time domain filters.

In the present paper, filters are used on two different occasions to suppress non SO-related variability in the data. Prior to the POP analysis a frequency domain filter is applied with the filter characteristic

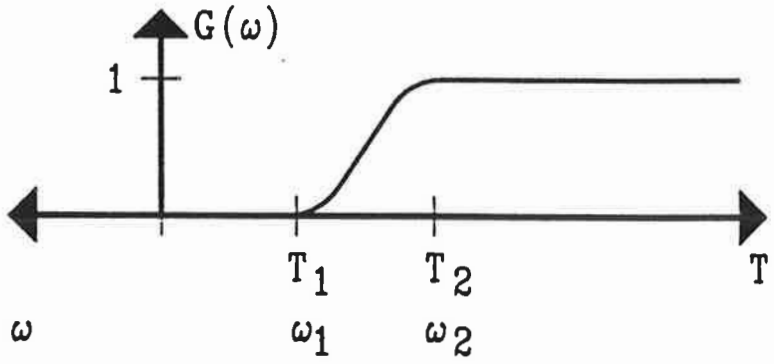

Figure A1:

Characteristic of the frequency domain filter used to suppress high frequency variations. For the details see text (Appendix).

$$H(\omega) = \begin{cases} 1 & 0<\omega \leq \omega_2 \\ 1/2\ [1-\cos(\frac{\pi}{\omega_1-\omega_2}(\omega-\omega_1))] & \omega_2 \leq \omega \leq \omega_1 \\ 0 & \omega > \omega_1 \end{cases}$$

with $\omega_1=(15 \text{ months})^{-1}$ and $\omega_2= (18 \text{ months})^{-1}$ (Figure A1). The smooth change from "no change" ($0<\omega\leq\omega_2$) to complete suppression ($\omega>\omega_1$) is introduced to avoid the generation of artificial secondary maxima due to "overshooting".

Because of the implicit assumption of periodicity the filtered time series is distorted at its ends, and also in the neighborhood of the break 1958/72. The distortion is limited to about ± 1 year of the discontinuity.

The use of a filter is also necessary when inferring the initial value and the most recent history to prepare a POP forecast. Since future values are not available, a time domain filter has to be used. To obtain maximum consistency with the POP analysis the frequency domain filter is approximated by a symmetric time domain filter with weights a_j. Since data are not available beyond the initial time, t_o, the filter has to be applied in non-symmetric mode:

$$\tilde{x}(t_o-k\Delta t) = \sum_{j=-m}^{k} a_j^* x(t_o+(j-k)\Delta t)$$

with $a_j^* = a_j \Big/ \sum_{j=-m}^{k} a_j$. This normalization of the filter coefficients, $\sum a_j^* = 1$, is introduced to enforce H(0) = 1. That is, the filter does not change the mean. The lack of symmetry introduces phase errors which are, however, largest for high frequencies (see A.2). Since these high frequencies are suppressed by the filter we found no significant distortions of the POP coefficient trajectories.

References:

Arkin, P.A., 1982: The relationship between interannual variability in the 200 hPa tropical wind field and the Southern Oscillation. - Mon. Wea. Rev. **110**, 1393-1404.

Barnett, T.P., 1984: Prediction of the El Niño 1982-83. - Mon. Wea. Rev. **112**, 1403-1407

Barnett, T.P., 1985: Variations in near-global sea level pressure. - J. Atmos. Sci. **42**, 478-501

Barnett, T.P., 1988: Variations in near-global sea level pressure: Another view. - J. Climate **1**, 225-230

Barnett, T; N.Graham; M.Cane, S.Zebiak; S. Dolan; J.O'Brien and D.Legler, 1988: On the prediction of the El Niño of 1986-87 - Science **241**, 192-196

Barnett, T.P.; L. Dümenil; U. Schlese, E. Roeckner and M. Latif, 1989: The effect of Eurasian snow cover on regional and global climate variations. - J. Atmos. Sci. **46**, 661-685

Battisti, D.S.; A. C. Hirst, 1989: Interannual variability in a tropical atmosphere-ocean model: Influence of the basic state, ocean geometry and nonlinearity. - J.A.S. **46**, 1687-1712.

Berlage, H.P., 1957: Fluctuations of the general atmospheric circulation of more than one year, their nature and prognostic value. - Koninklijk Nederlands Meteorologisch Instituut, Mededelingen En Verhandelingen, **69**.

Bjerknes, J., 1966: A possible response of the atmospheric Hadley circulation to equatorial anomalies of ocean temperature. - Tellus **18**, 820-829.

Bjerknes, J., 1969: Atmospheric teleconnections from the equatorial Pacific. - Mon. Wea. Rev. **97**, 163-172.

Blandford, H.F., 1894: On the connection of Himalayan snowfall and seasons of drought in India. - Proc. Royal Soc. London, **37**, 3-22.

Busalacchi, A.J., J.J. O'Brien, 1981: Interannual variability of the equatorial Pacific in th 1960's. - J. Geophys. Res., **86**, C11, 10901 - 10907.

Cane M., and S.E. Zebiak, 1985: A theory for El Niño and the Southern oscillation. - Science **228**, 1085-1087

Cane, M.,; S.E. Zebiak and S.C. Dolan, 1986: Experimental forecasts of El Niño. - Nature **321**, 827-832

Chu, P.S.; R.W. Katz, 1985: Modeling and forecasting the Southern Oscillation: A time-domain approach. - Mon. Wea. Rev. **113**, 1876-1888.

Gill, A.E., 1980: Some simple solutions for heat-induced tropical circulation. Quart. J. R. Met. Soc, **106**, 447-462.

Graf, H.F., 1989: Forced cooling of the polar T21 atmosphere and tropical climate variability - MPI Rep. **45**, Max-Planck Institut für Meteorologie, Bundesstrasse 55, 2000 Hamburg

Graham, N. E., J. Michaelsen, and T.P. Barnett 1987a: An investigation of the El Niño - Southern Oscillation cycle with statistical models. 1. Predictor field characteristics. - J. Geophys. Res. **92**, 14251-14270.

Graham, N. E., J. Michaelsen, and T.P. Barnett 1987b: An investigation of the El Niño - Southern Oscillation cycle with statistical models. 2. Model Results. - J. Geophys. Res. **92**, 14271-14289

Gutzler, D.S. and D.E. Harrison, 1987: The structure and evolution of seasonal wind anomalies over the near-equatorial Eastern Indian and Western Pacific Oceans. - Mon. Wea. Rev. **115**, 169-192

Hasselmann, K., 1988: PIPs and POPs: the reduction of complex dynamical systems using Principal Interaction and Oscillation Patterns. - J. Geophys. Res. **93**, 11015-11021

Hoskins, B., Karoly, 1981: The steady linear response of a spherical atmosphere to the thermal and orographic forcing. - J. Atmos. Sci. **38**, 1179-1196.

Inoue, M., and J.J. O'Brien, 1984: A forecasting model for the onset of El Niño. - Mon. Wea. Rev. **112**, 2326-2337

Kiladis, G.; H. Diaz, 1989: Global Climate Anomalies Associated with Extremes in the Southern Oscillation.

Kiladis, G.N., and H. van Loon, 1988: The Southern Oscillation. Part VII: Meteorological anomalies over the Indian and Pacific sectors associated with the extremes of the Oscillation. - Mon. Wea. Rev. **116**, 120-136

Latif, M.; E. Maier-Reimer; D.J. Olbers, 1985: Climate variability studies with a primitive equation model of the equatorial Pacific. In: J.C.J. Nihoul (Editor), Coupled ocean-atmosphere models. Elsevier, Amsterdam, 63-81.

Latif, M. 1987: Tropical ocean circulation experiments. J. Phys. Oceanogr., **17**, 246-263

Livezey, R., 1987: Caveat Emptor! The evaluation of skill in climate predictions. - in: Towards Understanding Climate Change (Ed.: U. Radok), Westview Press, Boulder, 149-177

Luksch, U.; H.v. Storch; E. Maier-Reimer, 1989: Modeling north Pacific SST anomalies as a response to anomalous atmospheric forcing. - MPI Report No.37 (Max-Planck Institut für Meteorologie, Bundesstrasse 55, 2000 Hamburg 13, FRG)

Mo, K.C.; H. van Loon, 1985: Climatic trends in the Southern Hemisphere. - J. Climate Appl. Met. **24**, 777-789

Mooley, D.; B. Parthasarathy, 1983: Variability of the Indian summer monsoon and tropical circulation features. - Mon. Wea. Rev., **111**, 967-978.

Preisendorfer, R.W., 1988: Principal Component Analysis in Meteorology and Oceanography - Elsevier Science Publishers, Developments in Atmospheric Sciences, 17, 426 pp

Rasmusson, E.M.; T.H. Carpenter, 1982: Variations in Tropical Sea Surface Temperature and Surface Wind Fields Associated with the Southern Oscillation / El Niño - Mon. Wea. Rev. **110**, 354-384

Ropelewski, C.F.; M.S. Halpert, 1987: Global and Regional Scale Precipitation Patterns Associated with the El Niño / Southern Oscillation - Mon. Wea. Rev. 115, 1606-1626

Shukla, J.; J.M. Wallace: Numerical simulation of the atmospheric response to equatorial Pacific sea surface temperature anomalies. - J.A.S. **40**, 1613-1630.

Storch, H.v.; T. Bruns; I. Fischer-Bruns; K.H. Hasselmann, 1988: Principal Oscillation Pattern analysis of the 30 to 60 day oscillation in a GCM. - J. Geophys. Res. **93**, 11022-11036

Storch, H.v.; H. van Loon; G.N. Kiladis, 1988: The Southern Oscillation: sensitivity to SST anomalies in the region of the South Pacific Convergence Zone. - J. Climate **1**, 325-331

Storch, H.v.; U. Weese and J. Xu, 1989a: Simultaneous analysis of space-time variability: Principal Oscillation Patterns and Principal Interaction Patterns with applications to the Southern Oscillation. - Proc. 4-th International Meeting on Statistical Climatology, Rotorua; also: MPI Report 34 (Max Planck Institut für Meteorologie, Bundesstraße 55, D 2000 Hamburg 13).

Storch, H.v; M. Latif; J. Biercamp, 1989b: Simulation of the Southern Oscillation in an general circulation model. - Phil. Trans. R. Soc. London A 329, 179-188

Storch, H.v. and J. Xu, 1989: Principal Oscillation Pattern analysis of the tropical 30- to 60-day oscillation. Part I: Definition of an index and its prediction. - MPI Report **43** (Max Planck Institut für Meteorologie, Bundesstraße 55, D 2000 Hamburg 13)

Suarez, M., and P.S. Schopf, 1988: A delayed action oscillator for ENSO. - J. Atmos. Sci., **45**, 3283-3287

Trenberth, K.E., and D.J. Shea, 1987: On the evolution of the Southern Oscillation. - Mon. Wea. Rev.**115**, 3078-3096

van Loon, H. and R. A. Madden, 1981: The Southern Oscillation. Part I: Global associations with pressure and temperature in northern winter. - Mon. Wea. Rev. **109**, 1150-1162

van Loon, H., 1984: The Southern Oscillation. Part III: Associations with the Trades and with the trough in the westerlies of the South Pacific Ocean. - Mon. Wea. Rev. **112**, 947-954

van Loon, H., K. Labitzke, 1987: The Southern Oscillation. Part V: The

anomalies in the lower stratosphere of the Northern Hemisphere in winter and a comparison with the Quasi-Biennial Oscillation. -Mon. Wea. Rev. **115**, 357-369

van Loon, H; D.J. Shea, 1985: The Southern Oscillation. Part IV: The precursors south of 15°S to the extremes of the oscillation. -Mon. Wea. Rev. **113**, 2063-2074.

van Loon, H; D.J. Shea, 1987: The Southern Oscillation. Part VI: Anomalies of sea level pressure on the Southern Hemisphere and of Pacific sea surface temperature during the development of a Warm Event - Mon. Wea. Rev. **115**, 370-379.

White, W.B.; S.E. Pazan and M. Inoue, 1987: Hindcast/forecast of ENSO events based on the redistribution of observed and model heat content in the western tropical Pacific. - J. Phys. Oceanogr. **17**, 264-280

Wright, P.B., 1984: Relationships between indices of the Southern Oscillation - Mon. Wea. Rev. **112**, 1913-1919.

Wyrtki, K., 1977: Sea Level During the 1972 El Niño. - J. Phys. Oceanogr. **7**, 779-787.

Wyrtki, K., 1979: The Response of Sea Surface Topography to the 1976 El Niño. - J. Phys. Oceanogr. **9**, 1223-1231.

Wyrtki, K., 1985: Water Displacements in the Pacific and the Genesis of El Niño Cycle. - J. Phys. Oceanogr. **90**, 7129-7132.

Zebiak, S.E.; M.A. Cane, 1987: A model El-Niño-Southern Oscillation. Mon. Wea. Rev. **115**, 2262-2278.